Volcanic spreading forcing and feedback in geothermal reservoir development, Amiata Volcano, Italia

Andrea Borgia[*†] **Alberto Mazzoldi**[*$], **Carlo Alberto Brunori**[+],
Carmine Allocca[*], **Carlo Delcroix**[*],
Luigi Micheli[#],
Alberto Vercellino[†], **Giovanni Grieco**[†],

[*] EDRA, via di Fioranello 31, 00134 Roma, Italia.
[$] UMSNH-IIM, Instituto de Investigaciones en Ciencias de la Tierra, Edif. "U" Ciudad Universitaria CP 58060, Morelia, Mich., México
[+] Istituto Nazionale di Geofisica e Vulcanologia, via di Vigna Murata 605, Roma, 00143 Italia.
[#] Regione Toscana, via di Novoli 26, Firenze, 50127 Italia.
[†] Dipartimento di Scienze della Terra, Università degli Studi di Milano, via Botticelli 23, Milano, 20133 Italia.

Corresponding author: Andrea Borgia, email: aborgia@lbl.gov

28 July 2014
Accepted by Journal of Volcanology and Geothermal Research

Abstract

We made a stratigraphic, structural and morphologic study of the Amiata Volcano in Italy. We find that the edifice is dissected by intersecting grabens that accommodate the collapse of the higher sectors of the volcano. In turn, a number of compressive structures and diapirs exist around the margin of the volcano. These structures create an angular drainage pattern, with stream damming and captures, and a set of lakes within and around the volcano. We interpret these structures as the result of volcanic spreading of Amiata on its weak substratum, formed by the late Triassic evaporites (Burano Anhydrites) and the Middle-Jurassic to Early-Cretaceous clayey chaotic complexes (Ligurian Complex). Regional doming created a slope in the basement facilitating the outward flow and spreading of the ductile layers forced by the volcanic load.

We model the dynamics of spreading with a scaled lubrication approximation of the Navier Stokes equations, and numerically study a set of solutions. In the model we include simple functions for volcanic deposition and surface erosion that change the topography over time. Scaling indicates that spreading at Amiata could still be active. The numerical solution shows that, as the central part of the edifice sinks into the weak basement, diapiric structures of the underlying formations form around the base of the volcano. Deposition of volcanic rocks within the volcano and surface erosion away from it both enhance spreading. In addition, a sloping basement may constitute a trigger for spreading and formation of trains of adjacent diapirs. As a feedback, the hot hydrothermal fluids decrease the shear strength of the anhydrites facilitating the spreading process.

Finally, we observe that volcanic spreading has created ideal heat traps that constitute todays' exploited geothermal fields at Amiata. Normal faults generated by volcanic spreading, volcanic conduits, and direct contact between volcanic rocks (which host an extensive fresh-water aquifer) and the rocks of the geothermal field, constitute ideal pathways for water recharge during vapour extraction for geothermal energy production. We think that volcanic spreading could maintain faults in a critically stressed state, facilitating the occurrence of induced and triggered seismicity.

Keywords

Amiata volcano; geology; structure; volcanic spreading; spreading model; geothermal traps formation.

1.0 Introduction

Spreading of volcanic edifices built on weak substratum is a well documented process (Borgia et al., 2000a). Numerous papers study this type of deformation, which is observed in the field (see for instance: van Bemmelen, 1949; Borgia et al., 1992; Merle et al., 1993; Merle et al., 1996; van Wyk De Vries and Borgia, 1996; Acocella et al., 2000; Neri et al., 2004; Rovida and Tibaldi, 2005; Mathieu and van Wyk De Vries, 2009) or measured via ground, air or space instruments (cf. Borgia et al., 2000b; Borgia et al., 2005; Solaro et al., 2010), or using analogue (cf. Merle and Vendeville, 1995; Merle and Borgia, 1996; van Wyk De Vries and Merle, 1996 and 1998; Acocella and Mulugeta, 2000; Wooller et al., 2004; Girard and van Wyk De Vries, 2005; Norini and Lagmay, 2005; Merle et al., 2006; Lagmay and Valdivia, 2006; Delcamp et al., 2008; Holohan et al., 2008; Le Corvec and Walter, 2009), numerical (cf. Borgia, 1994; van Wyk De Vries and Matela, 1997) or analytic (cf. Borgia et al., 2005; Borgia and Murray, 2010; Gudmunson, 2009; McGovern and Morgan, 2009; Plattern et al., 2013) experiments. To the best of our knowledge no work has been done on the structural consequences that spreading has on the development of geothermal fields associated with volcanic centres undergoing this process and on the feedback that geothermal fields can have on spreading.

We anticipate from the conclusions that volcanic spreading may creates heat-traps around the periphery of volcanoes and allowing efficient water recharge through extensional faulting of the edifices. In turn, the heat advected by the hydrothermal system may weaken the strength of rocks below the volcano facilitating spreading.

Amiata Volcano, located in southern Tuscany, Italy (Fig. 1), is an ideal example for the study of this process. On the one hand, the effects of volcanic spreading are quite evident, on the other, because of the largely exploited geothermal fields, the underground structures are particularly well defined.

After analysing in detail the volcanic succession, we describe the structural geology of Amiata Volcano focusing on the spreading process; then, we present a numerical solution of an analytic model for volcanic spreading of the Amiata edifice and, finally, we elaborate on the interactions between volcanic spreading and generation of geothermal fields.

2.0 Geology of the Amiata Volcano area

Detailed descriptions of the regional geology of the Amiata Volcano area may be found in Brogi (2008) and references therein and in the 1:10.000 Geologic Map of Amiata Volcano by Regione Toscana (2006-2009). Our survey has been limited to Amiata Volcano and the area around its periphery (Fig. 2). In brief, from Cretaceous to Oligocene, during the Apennine convergent orogenic tectonics, the Ligurian Units were thrust on top of the Sub-Ligurian Units (oldest-on-top-of-youngest); both of them were subsequently stacked on top of the Tuscan Units during Oligocene-Early Miocene. Post-collisional extensional tectonics, from Middle Miocene to Present, produced the collapse and thinning of the lithosphere and of the over-thickened crust associated with emplacement of plutons, uplift and, finally, during the Quaternary volcanic activity.

2.1 Stratigraphy

Brogi (2008), Regione Toscana (2006-2009) and references therein describe from bottom upward the following stratigraphic units in the Amiata Volcano area (Fig. 3):

a) The Paleozoic Gneiss upper crustal Complex (**GC**) is the lowermost known unit.
b) The Tuscan-Units Metamorphic Complex (**TMC**) is found only in boreholes and in xenoliths within the Mt. Amiata lavas. Locally this Complex is constituted of the very-low-grade metamorphic Monticiano-Roccastrada Units of Devonian-to-Triassic age that is further subdivided in three levels: the Micashists Group (**MS-TMC**), Phyllite-Quarzite Group (**PQ-TMC**) and the Verrucano Group (**VE-TMC**).
c) The Tuscan Units (**TU**) is related to the Late Triassic-Early Miocene sedimentary cover of the Adria continental paleo-margin. The Late-Triassic evaporites, the Anidriti of Burano (**AB-TU$_1$**), formed the detachment above which the Tuscan Units were trust over the outer paleogeographic domain during Late Oligocene-

Early Miocene. Above the evaporites, the rocks are mainly carbonates and turbiditic units (**LT-TU$_2$**).

d) The Subligurian Units (**SL**) of Eocene to Oligocene age are a sedimentary domain interposed between the Tuscan and Ligurian domains and are locally represented by the Canetolo Sandstone (**CA-SL**).

e) The Ligurian Complex, of Middle Jurassic to Early Cretaceous age is composed of remnants of the oceanic basement and its sedimentary cover and is subdivided in External Ligurids (**EL**) – including Argille Varicolori (**AV-EL**), Santa Fiora Unit (**SF-EL**), and Pietraforte (**PF-EL**) of Early Cretaceous to Eocene age –, and Internal Ligurids (**IL**) – composed by the ophiolitic olistostrome of the Argille a Palombini Formation (**AP-IL**) of Cretaceous age.

f) The Pleistocene Intrusive Complex (**IC**) is constituted by the intrusive rocks that form the Mount Amiata magma chamber and the Selagites (**SE**) that are constituted by lamprophires, minettes, spessartites, componites, lamproites, etc. (Regione Toscana 2006-2009).

g) The Mt. Amiata Volcanic Complex (**VC**; also surveyed in this work), is constituted by at least 16 morphologically-distinct lava-flow units of dacitic, rhyodacitic and olivine-latitic composition. The lavas, erupted 300-200 ka B.P., contain mafic enclaves (Ferrari et al., 1996; Cadoux and Pinti, 2009).

h) Miocene-to-Quaternary marine and continental sediments (**M-P-Q**) include alluvial (al) and travertine (tr) deposits.

Detailed cross-sections of Amiata mines (Ref. AAVV, 1971) combined with a large number of boreholes (Archives of AVAM) show that the Amiata volcanic units are, on its eastern side, in direct contact with the calcareous sequence of the Tuscan Units (Fig. 4a), a fact that apparently was neglected in the recent literature (cf. Doveri et al., 2012). Because the Tuscan Units have high secondary permeability – they are highly tectonized –, they constitute (in addition to faulting and volcanic conduits) preferential pathways for the interaction between freshwater and geothermal fluids.

Using aerial photographs, the newly-produced geologic map of the Amiata Volcanic area (Regione Toscana, 2006-2009) and extensive field controls (Delcroix et al., 2006; this work) we carried out a detailed reconstruction of individual Amiata Volcano lava domes, coulees and flows and of the sedimentary volcanic basement

cropping out in the surrounding area (Fig. 2). The reconstruction of lava units is more reliable for the younger flows, while it has a larger degree of error for the older ones, where the gravitational deformation has been so extensive that, apart from a few cases, it is now difficult to indicate their flow directions, extent and source as these older flows are also indistinguishable in geochemistry, mineralogy or age (Ferrari et al., 1996).

Lava domes are frequently stratified, indicating subsequent eruptive pulses in their formation (exogenous domes). Some flows are un-rooted and appear to have originated from lava fountains or strombolian activity that accumulated large cones of hot-lava debris, part of which, in turn, flowed downward or collapsed, possibly giving rise to hot-avalanches. Using the superposition criteria, we have detailed the volcanic stratigraphy, reconstructing a preliminary time succession of 16 flow units that form the complete life of the volcano. These volcanic units have been dated at 0.3 and 0.2 Ma BP (Ferrari et al., 1996; Cadoux and Pinti, 2009, and references therein), although the surface blocky morphology of the youngest flow, practically lacking soil cover, suggests a much younger age.

Tephra layers are practically absent from the sequence at Amiata volcano. This fact is at odds with all the other volcanoes of the Latium-Campanian volcanic chain, which show extensive deposits formed by ultra-Plinian, Plinian, and sub-Plinian eruptions. A number of depressions, bound by normal faults and/or by back-sloping lavas have allowed the formation Lacustrine deposits ("lac" in Fig. 2), often constituted by diatomites, iron oxides and amorphous silica (De Castro, 1914; Pompei, 1924; Fig. 4b).

2.2 Structure

2.2.1 Compressional and extensional tectonics

Brogi (2008) and references therein report that during orogeny, from Cretaceous to Early Miocene, the Tuscan Units became intersected by major E-verging thrust faults accompanied by a set of recumbent folds having N-S fold axes. A second set of asymmetric, overturned, E-SE-verging folds with axial planes that dip NW were formed during Early(?)-Middle Miocene. Low-angle, N-S-trending, E-dipping, normal faults delaminated the former stacked Units during Middle and Upper

Miocene, producing strong variations in their thicknesses. At the base of the Tuscan Units, these normal faults flatten out in a decollement constituted by the Triassic Burano Anhydrites. Additional clayey-rich detachment layers are found between the Tuscan and the Sub-Ligurian Units, the Sub-Ligurian and the Ligurian Units, and also within the Ligurian Units themselves (Fig. 3). A younger set of Early Pliocene to Quaternary, steeply dipping, NNW-SSE and ENE-WSW striking normal faults dissect the older structures in the Amiata Volcano area. Where observable, these faults frequently show both left-lateral and right-lateral component of slip, but they were ultimately reactivated as normal faults particularly in proximity of Amiata Volcano (Brogi and Fabbrini, 2009). It appears that this normal faulting occurred during the Pliocene intrusive activity and the associated gravimetric adjustments of the volcanic products (Brogi and Fabbrini, 2009). The ENE-WSW striking normal fault is the one that focused volcanic activity at Amiata.

Baietto et al. (2008), through detailed analyses of structural stations both on Amiata Volcano and on the neighbouring outcrops, found that the area is characterized by strike-slip faulting younger than the emplacement of the volcanic rocks ($<2*10^5$ a BP). Main transtensional faults through the volcano strike E-W and have a right-lateral sense of shear, whereas in the northeastern sector NE-SW striking transtensional faults have left-lateral sense of shear. Normal faults trend NW-SE; southwest away from the edifice of Amiata these faults have down-throws to the SW, while NE of Amiata they have down-throws to the E.

Brogi et al. (2010) suggest that the above-mentioned ENE-WSW-striking normal fault cutting the volcano is a left-lateral strike-slip fault that cuts through the volcano and its substratum, extending also to the NE and SW away from it. In the NE area right-lateral strike-slip faults are interpreted to form a step-over releasing-band of the main left lateral strike-slip faults; in addition, the mutual overlap of transtensional and near normal kinematic indicators, often observed on the shear surfaces, suggests reactivation of the pre-existing fault planes in an extensional context. In the SW, the SW-NE left lateral fault divides two domains: the northern one characterized by normal faults, and the southern one by right-lateral faults at low angle with the master left-lateral fault. Within the volcano the examined mesostructures are minor faults

with associated joints and few kinematic indicators (rare mechanic striations, lunate structures, and pinnate joints probably associated with shear fractures).

We observed that the left- versus right-lateral strike-slip kinematic indicators presented in the former papers (Brogi, 2008; Baietto et al., 2008, Brogi et al., 2010), appear to be in contrast with each other if related to regional tectonics. In the NE the proposed left-lateral strike-slip fault in the travertine is a pure extensional fracture probably related to sagging and slumping of the travertine over the underlying shaley Ligurid Units (Fig. 5). In the SW the proposed normal faulting may be more reasonably interpreted as a NW-SE series of faults related to diapirism that involves the basal lava flows of Amiata (cf. also Betz, 1962).

In addition, we believe that the striations and kinematic indicators found on fault planes within the Amiata Volcano lavas could receive different explanations from the one reported in the cited papers. In fact, both, the mechanism of lava flow emplacement (Fink, 1980; Leat and Schminke, 1993; Linneman and Borgia 1993; Tibaldi, 1996) and volcanic spreading (Monaco et al., 1997; Solaro et al., 2010) can create a wide range of structures that are identical to those created by regional strike-slip tectonics and that can extend well beyond the volcanic products (see for instance Borgia et al., 1992; Borgia and van Wyk De Vries, 2003, Solaro et al., 2010). Actually, on volcanoes, the most reliable kinematic indicators are the offsets of the isochrone surfaces identified by individual flows. These are the indicators we have used for our structural mapping.

We do not claim, though, that strike-slip regional components to the spreading process is absent for sure. In fact, some morphologic features along the volcanic axis could suggest the existence of small regional components of shear (perhaps right lateral), overprinting the general spreading process (cf. Lagmay and Valdivia, 2006). Future work will attempt at verifying this thesis.

2.2.2 Regional intrusion, uplift and volcanism

Acocella (2000) and references therein point out that the rapid Quaternary uplift and the bedding orientation of the Pliocene sediments define a broad regional dome,

256 centered on the Mt. Amiata Volcano, which was generated after the emplacement of
257 an intrusive body at depth. This intrusion is thought to be responsible for the Middle-
258 Quaternary volcanic activity.
259
260 Batini et al. (2003) indicate that a seismic horizon (K-horizon) exists at depth. It has
261 an antiformal structure elongated NE-SW, parallel to the volcano axis, from 4 km b.s.l
262 under the volcano, to about 8 km b.s.l. at a distance of about 10 km NW and SE from
263 it. This horizon is interpreted to be an active shear-zone with high fluid-pore pressure,
264 located at the brittle-ductile transition (Gianelli et al., 1997; Liotta and Ranalli, 1999).
265 Brogi (2008) shows that the K-horizon is mimicked by the bottom of the Triassic
266 evaporite (AB-TU_1, at the top of the Tuscan Metamorphic Complex, TMC), which is
267 found at sea level under the volcano and at more than 3 km b.s.l. at a distance of about
268 10 km NW from it (Fig. 6). Toward the SE this horizon is less inclined reaching 1.5
269 km b.s.l. at about the same distance.
270
271 *2.2.3 Diapirism*
272 Clayey diapirs occurring in the area across the margin of the volcanic sequence have
273 hardly received attention. Our work show, in fact, that they occur at all scales:
274 a) At the largest scale (0.1 to 10 m), clay sediments intrude the oldest lava
275 sequences forming dikes from a few decimeters to many meters in thickness
276 (Fig. 7). This phenomenon, similar to what has been found at Conception
277 Volcano in Nicaragua (Borgia and van Wyk De Vries, 2003), occurred during
278 flow emplacement or shortly thereafter, because the clay in the dikes has
279 turned red by heating from the flows (also cf. Bertini et al., 2008). In addition,
280 to allow intrusion, the clays should have been still unconsolidated. These
281 observations suggest that some of the flows could have been emplaced in a
282 lacustrine environment.
283 b) At the middle scale (10 to 100 m), clayey diapirs, both from chaotic
284 Pietraforte and Argille a Palombini formations, extend and dismember the
285 overlying lava flows turning them into meter-size lava-block fields (Fig. 2). In
286 some cases, as at Ermicciolo in the NE part of the volcano, the diapirs seem to
287 pierce the flows, providing the impermeable base for emerging springs.

c) At the smallest scale (100 m to 1 km) clayey diapirs rising at the edge of the volcano are thrust over lava blocks at the outer margin of the volcano (Fig.s 8 and 4c). Clayey diapirs also occur within the Ligurian units in a belt northwest and west of the base of Amiata. Here the stratigraphic lower Sub-Ligurid unit (**CA-SL**) and the External Ligurid (**AV-EL**) rise with tectonic contacts into the upper External Ligurid (**PF-EL**) and Internal Ligurid (**AP-IL**) units (Fig. 2-geology; Fig. 6b). In addition, around the periphery of the volcano, the lava flows become uplifted and tilted toward the volcano forming gentle synclines (also cf. Ferrari et al., 1996), which, in turn, are frequently filled with lake sediments (Fig. 2). Finally, anhydrite diapirs rise forming doming structures into the Tuscan and Ligurid Units in a belt around to the base of Amiata (Fig. 6a). SE and SW of Amiata Volcano, where the anhydrites domes (which are permeable due to fracturing and dissolution processes) are covered by the clayey Ligurid Units, they form ideal high-temperature geothermal heat traps. Indeed, these are the location of the historically exploited geothermal fields. In the NE, instead, where the Ligurian Units have been eroded away, and the rocks of the geothermal field crop out, the rising geothermal fluids feed historically-known low-temperature hot springs.

2.3 Geomorphology

We have done a detailed analysis on river and stream flow directions. In principle, with no tectonic influence, streams should have a general radial pattern away from the upper part of the volcano (apart for the case of domes growing inside a valley). Therefore, anomalous sharp changes in flow directions, relative to this pattern could be the consequence of tectonic activity. Our analysis shows that both within and outside the volcano a set of sharp changes in the flow directions from the radial pattern is indicative of strong structural control on surface-water flow-directions. Within the volcano, radial steepest-descent flow-directions are cut by ridges that abruptly divert rivers and streams, which become tangential to the volcano (Fig. 9a). Away from the volcano, additional ridges divert the flow of streams (Fig. 9b) forming entrenched streams, stream captures, and hanging and dammed valleys. These morphologic features occur because of normal faulting (Losacco, 1957; Ferrari et al.,

1994), which downthrow the central part of the volcano relative to the margins, and of thrusting and diapiric faulting in a belt around the base of the volcano.
We interpret these features as the result of radial outward spreading of the anhydrites formation and of the chaotic shaley units (Ligurid Units) under the load of the volcano.

2.4 Volcanic spreading

The first suggestion on the existence of gravitational tectonics on the Mt. Amiata region was made by Cataldi (1965). In particular, he suggests that the diapiric deformation, which originates in the evaporitic Triassic formation cut upward into the clayey formations of the Tuscan and Ligurian Units, forming in some places, like at Poggio Zoccolino NE of Amiata, structures that can be classified as "piercing" tectonic features (Fig. 6a). He also pointed out that the structures within the evaporites and the overlying clayey units are in part independent from the structures of the underlying metamorphic basement. The faults that affect the evaporitic formation cut upward into the clayey formations disrupting and thinning them, thus, creating localized section of higher permeability. Cataldi (1965), though, attributes these gravitational tectonic events to pre-volcanic times.

Calamai et al. (1970) show that positive and negative tectonic features on top of the evaporitic formation generally trend N-S. However, as they approach Amiata Volcano, these features are rotated, becoming tangential all around the volcanic edifice, and are displaced by volcano-tectonic faulting. Although most of the deformation is considered to be pre-volcanic, volcano-tectonic faulting is then supposed to have influenced locally the recent tectonics. In particular, it was observed that the volcanic edifice is normally faulted and sank into its basement. The basement itself below the volcano forms a closed depression bounded by volcano-tectonic normal faults. In addition, a set of faults are concentric to Mt. Amiata with the up-thrown block on the volcano side; these faults run all the way from north of Poggio Zoccolino with NE strike passing to the east to a SE strike, to north of Abbadia San Salvatore with a SSE strike, to south of Abbadia with SSW strike, to south of Piancastagnaio with a WSW strike. This fault-set diverges substantially from the N-S trend of the regional Pleistocene set of faults of the Radicofani graben. Our work

353 shows that at the surface this fault-set corresponds to topographic ridges, concentric to
354 the volcano, which divert the drainage pattern, constituting the external boundary of
355 the geothermal fields and of the Selagites outcrops.
356
357 We suggest that these faults are the expression of diapiric thrust fronts generated by
358 the gravity spreading of the volcanic edifice. We point out that in many of the
359 volcanoes, where spreading has been recognized, these thrusts have been first
360 interpreted as normal faults, such as the Central Costa Rica Volcanic Range and
361 Kilauea volcano (Borgia et al., 1990), Etna Volcano (Borgia et al., 1992), and
362 Concepciòn Volcano (Borgia and van Wyk de Vries, 2003).
363
364 Canuti et al. (1993), Ferrari et al. (1996), and later Garzonio (2008) suggest the
365 existence of deep-seated gravity deformation on Amiata volcano. Based on a
366 stratigraphic and structural study, Ferrari et al. (1996) try to correlate the normal
367 upward-facing faults within the volcanic edifice with the rotation of regional fold
368 axes, which become tangential to the northern and southern base of Amiata. Volcanic
369 loading would, therefore, produce collapse and spreading of the central part of the
370 volcano with consequent compression at its base.
371
372 Bonini and Sani (2002), and Bonini et al. (2014) show in a number of seismic lines,
373 striking ENE across the Radicofani Graben just west of the Amiata Volcano, small
374 thrust faults cutting the Plio-Pleistocene marine deposits with hanging-wall motion
375 toward the ENE, that is away from the volcano. Brogi (2008) indicates that these
376 thrust faults could be better explained by gravitational rather than regional tectonics.
377
378 Part of this basal deformation is also indicated in the structural maps of Calamai et al.
379 (1970) and Acocella (2000) where a relatively large number of NNW-SSE trending
380 short-wavelength folds and thrust faults intersect the Plio-Pleistocene Marine deposits
381 at the eastern base of Amiata Volcano. We observe that these folds and faults do not
382 appear to continue north and south of the Volcano, suggesting a direct relation with it.
383
384 Our reconstruction of flow surfaces (Fig. 2) shows that most of the volcanic edifice is
385 cut by faults mainly with downthrown blocks toward the volcano summit, a fact that

has been documented also in previous studies (Calamai et al., 1970; Ferrari et al., 1996). Although normal faulting within the volcano tends to have a prevailing NE-SW strike, we identify also leaf-grabens and wedge-horsts similar to those found on Etna (Merle and Borgia, 1996) or Vesuvius (Borgia et al., 2005). The collapse of the central part of the volcanic edifice and its sinking in the anhydrites and shaley formations induced their radial flow toward the periphery giving rise to volcanic spreading (Fig.s 2c and 6a). In turn, the anhydrites and clayey formation around the base of the volcano were involved in diapiric-like tectonics, dismembering the distal sections of the flow fields (Fig.s 2a and 6) and diverting and damming the drainage (Fig. 9).

We suggests that volcanic spreading at Amiata occurs on the weak substratum constituted by the late Triassic evaporites (Burano Anhydrites) and the Middle-Jurassic to Early-Cretaceous clayey chaotic complexes (Ligurian Complex). Because of these, the anhydrites have been "squeezed out" from below and have accumulated in domes and diapirs at the base of the volcano. Since these domes have a shaley cover (cap rock), they form ideal heat traps for geothermal fields. In turn, the ductile deformation of the evaporites has been drastically enhanced by the high-temperature hydrothemal fluids of Amiata Volcano. In fact, the plastic strength of anhydrites decreases by more than two orders of magnitude as the temperature increases above 120 °C (Suppe, 1985). In addition, regional doming (Acocella, 2000) creates a basement that slopes away from the volcano, boosting even more the outward flow and spreading of the ductile layers below the load of the volcano.

Finally, we speculate that the absence of tephra layers from the sequence at Amiata volcano could also result from volcanic spreading. In fact, by decreasing the lithostatic pressure on the magma, volcanic spreading allows magma degassing over long periods of time inhibiting gas-phase pressure build up and, in turn, energetic explosive activity. The same mechanism has also been proposed for Conceptión in Nicaragua (Borgia and van Wyk De Vries, 2003) and Vesuvius in Italy (Borgia et al., 2005).

3. Dynamics

In order to model the deformation structures found in the field we conceptualize Amiata volcano as a brittle cone above a viscous substratum. The cone is made of volcanic rocks, while the substratum consists of the clayey Ligurid complexes and the underlying Anhydrite Formation (Fig. 10).

3.1 Analytical model

The deformation of a thin ductile layer under the differential loading induced by the topographic relief of the volcano may be described by the lubrication approximation of the Navier Stokes equations (Bird et al., 1960; Borgia et al., 2006), which in 2-D rectangular coordinates can be written as:

$$\left\{\begin{array}{ll} \dfrac{\partial v_x}{\partial x}+\dfrac{\partial v_z}{\partial z}=0 & \text{mass conservation} \quad (1a) \\ -\dfrac{\partial p}{\partial x}+\mu_d\dfrac{\partial^2 v_x}{\partial z^2}+\rho_d g\sin\alpha=0 & \text{x-momentum conservation} \quad (1b) \\ -\dfrac{\partial p}{\partial z}-\rho_d g\cos\alpha=0 & \text{z-momentum conservation} \quad (1c) \end{array}\right\}$$

where x is the distance from the centre of the volcano along the top of the rigid substratum, that slopes with an angle α; z is the vertical coordinate, positive upward; p is pressure; g is the gravity acceleration; the ductile layer has a viscosity μ_d and a density ρ_d; v_x and v_z are the components of the velocity in the x and z directions, respectively.

For no-mass generation, the boundary conditions (BC) for Eq. (1a) are

$$v_z\big|_{z=0}=0 \qquad (2a),$$

$$v_z\Big|_{z=h_d}=\int_{v_z|_{z=0}}^{v_z|_{z=h_d}}\partial v_z=\frac{\partial h_d}{\partial t} \qquad (2b).$$

While the first of these two equations implies no slip at the lower boundary, the second indicates that the deformation of the top of the ductile layer follows the time (t) evolution of its thickness $h_d(x, t)$. The condition for Eq. (1b) is for no slip at the lower boundary

$$v_x\big|_{z=0}=0 \qquad (2c).$$

The upper BC, for $\alpha>0$ and no-slip between ductile and brittle layers, is determined by the behaviour of the brittle layer at the scale of the system. There can be three limiting cases:

1) for the case of a total laterally constrained brittle layer, the BC is (Borgia et al., 2000)

$$v_x\big|_{z=h_d} = 0 \qquad \text{(2d1)};$$

2) for the case of an upper brittle layer that is carried passively on top of the ductile layer, the top BC is

$$\frac{\partial v_x}{\partial z}\Big|_{z=h_d} = 0 \qquad \text{(2d2)};$$

3) finally, for the case of an unconstrained brittle layer, the top BC is determined by the x-component of the load of the layer (Borgia et al., 2002), that is

$$\frac{\partial v_x}{\partial z}\Big|_{z=h_d} = -\frac{\rho_b g h_b \sin\alpha}{\mu_d} \qquad \text{(2d3)},$$

which reduces to Eq. (2d2) for $\alpha = 0$.

The condition for Eq. (1c) is hydrostatic pressure given by:

$$p\big|_{z=h_d} = P_b(x,\, t) = \rho_b g h_b \cos\alpha + P_0 \qquad \text{(2e)},$$

where $h_b = h_b(x, t)$ and ρ_b are, respectively the thickness, a function of x and t, and the density of the brittle layer; P_0 is the atmospheric pressure and is assumed constant. Since pressure is a scalar, this condition also solves implicitly the pressure boundary condition in Eq. (1b).

Integrating Eq. (1) with the given BC, leads to:

$$\frac{\partial h_d}{\partial t} = \frac{\rho_d g \cos\alpha}{3c\mu_d}\frac{\partial}{\partial x}\left\{h_d^3 \frac{\partial}{\partial h}\left[h_d + \left(\frac{\rho_b}{\rho_d}\right)h_b\right] + \tan\alpha\left[d\,\frac{3}{2}\left(\frac{\rho_b}{\rho_d}\right)\frac{h_b}{h_d} - 1\right]\right\} \qquad \text{(3a)},$$

where the constants c and d, in accordance with the different BC, take the following values:

$c = 4$ and $d = 0$ for the 1st type of BC - Eq. (2d1) (3b),

$c = 1$ and $d = 0$ for the 2nd type of BC - Eq. (2d2) (3c),

$c = 1$ and $d = 1$ for the 3rd type of BC - Eq. (2d3) (3d).

To make Eq. (3a) dimensionless and scaled, we assume the following variables:

$$\xi = \frac{x}{R_v} \qquad \text{(5a)},$$

$$\eta = \frac{h_d}{H_d} \quad (5b),$$

$$\varphi = \frac{h_b}{H_b} \quad (5c),$$

$$\tau = \frac{t}{T} \quad (5d).$$

In Eq. (5a), R_v is the characteristic length of the topography in the x-direction, that is the radius of the volcano. In addition, for a small angle α, the topography is the major forcing function onto the system. Therefore, R_v should become also the characteristic length of the ductile layer, that is $L_d = R_v$. For the thicknesses (Eqs. 5b and 5c) we have three scaling variables H_d, H_b and H_v that are, respectively, the maximum thicknesses of the ductile and brittle layers at the start of the process and the height of the volcano. Since (H_d /H_v) and (H_b /H_v) are constants, these scaling variables may be used interchangeably. T is the characteristic time of evolution of the system (Eq. 5d).

Substituting these variables into Eq. (4), leads to:

$$\frac{\partial \eta}{\partial \tau} = \frac{\partial}{\partial \xi}\left\{\eta^3\left[\frac{\partial}{\partial \xi}\left(\eta + f\varphi\right) + r\left(d\frac{3}{2}\frac{f\varphi}{\eta} - 1\right)\right]\right\} \quad (6a),$$

where

$$T = \frac{3c\mu_d H_v^3}{\rho_d g \cos\alpha R_v^2} \quad (6b).$$

$$f = \frac{\rho_b H_v}{\rho_d R_v} \quad (6c),$$

and

$$r = \frac{\tan\alpha}{H_d / L_b} \quad (6d),$$

On the right side of the equal sign in Eq. (6a) within the square brackets of Eq. (6a), the left term $\frac{\partial}{\partial \xi}\left(\eta + f\varphi\right)$ describes the flow induced by the hydrostatic pressure within the ductile layer – which, in turn, is controlled by the topography of the volcano; the right term $r\left(d\frac{3}{2}f\frac{\varphi}{\eta} - 1\right)$ accounts for the flow induced by the

component of gravity in the x-direction: the first of the two terms in parenthesis is the contribution of the brittle layer, the second that of the ductile layer.

Since the left term within the square brackets of Eq. (6a) is of order 1, that is

$$\frac{\partial \eta}{\partial \xi}\left(\eta + f\varphi\right) = O(1) \qquad (7),$$

there can be three possibilities:

1. $r << 1$ (8a1),

that is for small slopes $\tan\alpha$ is small relative to H_d/L_b. Therefore, Eq. (6a) reduces to the equation used by Borgia et al. (2000) and Borgia et al. (2003)

$$\frac{\partial \eta}{\partial \tau} = \frac{\partial}{\partial \xi}\left[\eta^3 \frac{\partial}{\partial \xi}\left(\eta + f\varphi\right)\right] \qquad (8a2).$$

2. $r = O(1)$ (8b),

for which both terms in Eq. (6a) are relevant and is used the full Eq. (6a). Finally,

3. $r >> 1$ (8c1),

which implies that for large slopes $\tan\alpha$ is large relative to H_d/L_b and Eq. (6a) reduces to

$$\frac{\partial \eta}{\partial \tau} = r\frac{\partial}{\partial \xi}\left[\eta^3\left(d\frac{3}{2}\frac{f\varphi}{\eta} - 1\right)\right] \qquad (8c2).$$

If we now assume that the thickness of the brittle layer (that is the volcanic edifice and the surrounding topography) can be represented by the following simple function

$$h_b = H_v e^{-\frac{x}{R_v}} + x\tan\beta + b \qquad (9),$$

where β is the angle of regional topographic slope relative to the rigid basement, R_v is the geometric radius of the volcano of height H_v obtained by interpolating the topography (in model coordinates) to Eq. (9), and *b* is the minimum thickness of the brittle layer. In dimensionless form we may write:

$$\varphi = e^{-\xi} + s_1\xi + s_2 \qquad (10a);$$

where

525 $$s_1 = \frac{\tan\beta}{H_v / R_v} \quad (10b),$$

526 $$s_2 = \frac{b}{H_v / R_v} \quad (10c).$$

527

528 We remark that the scaled thickness of the brittle layer $\varphi = \varphi(\xi, \tau)$ is a function of the
529 scaled horizontal dimension and time. That is Eq. (10a) can include the time and
530 space functions of volcano growth and surface erosion.

531

532 Ideally, the coefficients in Eq. (10a) should be obtained from interpolating this
533 equation to the actual thickness of the brittle layer before deformation begins. In
534 practice, for a deformed volcano such as Amiata, we know this thickness only well
535 after deformation has started, and possibly well after deformation has ended.

536

537 *3.2 Scaling analysis*

538 Table 1 contains the values for the parameters used in our scaling analysis and in the
539 numerical solution of Eq. 6. These values are taken directly from measurements of
540 morphologic features and geometry of Amiata Volcano and from the bibliography.

541

542 The time scale for deformation, given by Eq. (6b), is in the order of magnitude 350 ka
543 for the first type of boundary condition decreasing by about 4 times to 90 ka for the
544 second and third type of boundary conditions. This is an important finding because, if
545 the 1st type of BC is the one that actually represent the real condition, the
546 corresponding time scale is larger than the age of Amiata (about 300 ka), indicating
547 that volcanic spreading (deep-seated gravity deformation) may still be active.
548 However, if the 2nd or 3rd types of BC are applicable, the spreading may well be
549 ended.

550

551 It is also possible that different BC are applicable to different sectors of Amiata,
552 making the deformation active only in some of these sectors. Even if we are not able
553 to unambiguously demonstrate this at present, our fieldwork suggests that spreading
554 of the northern sectors of Amiata is probably ceased, while it is still probably active
555 on the southern sectors.

From Eq. 6b we may write

$$H_v = \sqrt[3]{\frac{3c\mu_d}{\rho_d g \cos\alpha T}} R_v^{2/3} \approx 4R_v^{2/3} \qquad (11).$$

Borgia and Murray (2010) have shown that the fraction under the cube root on the right of the equal sign tends to be constant, with an approximate value of 4. Therefore, Eq. 11 gives a direct relationship between heights and radii of spreading volcanoes. Fig. 11 shows that Amiata Volcano fits this criteria, standing at the lowest (and smallest) end of our list of spreading volcanoes.

3.3 Numerical solution

We solve Eq. (6) numerically using Mathematica™ with a thickness of the brittle layer (the surface topography) as a function of ξ and τ given by Eq. (10) that also gives the topography at time zero. The solution is explored for the three BC given in Eq. (7), for basement slopes of 0° and 5°, and for a surface topography that varies in space and time. We simulate a total of 12 independent conditions (Table 2).

This set of conditions actually represents a larger set of 24 scenarios of which 12 give identical solutions. In particular, the solutions given by the 1st type of BC (Eq. 7a) are identical to those obtained by the 2nd type of BC (Eq. 7b); the only difference being the value of the dimensionless scaled time, which is four times larger for the 1st (c = 4) relative to the 2nd (c = 1) type of BC. For the 3rd type of BC the solutions are equal to those generated by the 1st type only for the case of a horizontal basement ($\alpha = 0°$).

The surface topography is modelled in a very simple fashion. We choose to stress the importance of topographic evolution in determining ductile-layer deformation, more than trying to simulate the actual changes of topography for which we have at the moment no data. We make surface topography evolve according to a function that depends on different degrees of lava emplacement on the volcano and surface erosion away from it. We observe that as the volcano and its substratum sink into the ductile layer, new lava flows may be emplaced that compensate to a given degree the rate of sinking. Similarly, away from the volcano, as the surface topography is lifted up or

588 subsides there is respectively either erosion or deposition that will also compensate to
589 a given degree the ductile-layer deformation. In practice we use a multiplayer
590 constant – which we call coefficient of topographic recovery (e) – to simulate the
591 recovery of different amounts of topographic changes. This constant equals zero to
592 simulate no deposition (lava flows and sediments) and erosion (sediments); it is one to
593 simulate a topography that is maintained at constant elevation by deposition and
594 erosion processes. We have also set this constant to 0.25 and 0.50 to simulate
595 intermediate conditions in which the original thickness of the brittle layer is recovered
596 only by a fraction.
597
598 Fig. 12 shows the results for the cases discussed above. It can be observed that, as the
599 slope angle increases, the effect given by x-component of the load onto the ductile
600 layer increases accordingly, giving rise to waves that tend to have larger amplitudes
601 closer to the volcano base. Also, as the deposition/erosion effect increases, so does
602 the diapiric effect in the ductile layer. The combination of larger slopes, third type of
603 boundary condition and maximum deposition/erosion effect makes the numerical
604 solution to Eq. (6a) evolve to a singularity as the rising diapir of ductile layer pierces
605 the topography closer to the volcano.
606
607
608 **4. Summary of conclusions**
609 Our detailed straigraphic, structural and morphologic study of Amiata Volcano shows
610 that volcanic spreading has profoundly dissected its edifice, creating a set of summit
611 grabens, flank-displacement structures and basal diapiric and thrust structures that
612 differ substantially from caldera-type collapse structures (Fig.s 2 and 6). These
613 structures have profoundly affected the drainage pattern, which is now strongly
614 angular, streams dams and capture (Fig. 9), and a set of lakes within and around the
615 volcano.
616 Our thesis agrees with the conclusions of former works on the tectonics of Amiata by
617 Ferrari et al. (1996) and Garzonio (2008), but disagrees with the work of Brogi et al.,
618 (2010), which proposes that the deformation of the Amiata volcanic edifice is due to
619 left-lateral strike-slip regional tectonics. We find little evidence of active strike-slip
620 regional tectonics on Amiata, although this kind of tectonics could certainly have

been active at an earlier time to trigger magma ascent and eruption. We think that most of the strike-slip indicators found on Amiata Volcano lavas are the result of differential motions occurring between adjacent lava flows sections, similar to what has been demonstrated to occur on lava flows at many other volcanoes (Fink, 1980; Leat and Schminke, 1993; Linneman and Borgia 1993; Tibaldi, 1996), or between adjacent spreading sectors (Borgia et al., 1992).

We propose that volcanic spreading has forced the flow of the anhydrites toward the periphery of the volcano and their diapiric rise around its base. Where present, the impermeable shaley cover formed by the Ligurian Units has allowed the formation of geologic traps where the hydrothermal circulation have accumulated heat to form ideal surficial high-temperature geothermal fields. In turn, the high temperature lowered the viscosity of the anhydrites enhancing the spreading process. The shaley chaotic complexes have facilitated the deep-seated gravitational deformation of the volcanic edifice to a smaller percentage.

Our analytical scaled model, based on the lubrication approximation of the Navier-Stokes equations, suggests that spreading occurs over a time that ranges between 50 ka and 500 ka, suggesting that spreading may still be active (Fig. 11). Also, basement slope (Woller et al., 2004), lava deposition on the volcano and surface erosion away from it can enhance the spreading dynamics creating radial train of diapirs (Fig. 12).

Finally, the normal faults generated by volcanic spreading and the volcanic conduits, in addition to the direct contacts between the volcanic rocks and the rocks of the Tuscan Formation that host the geothermal fields, constitute undoubtedly ideal paths for water recharge during vapour extraction for geothermal energy production. In this context, if volcanic spreading is still active, as the scaling analysis suggests, it could maintain faults in a critically stressed state, facilitating the occurrence of seismicity induced or triggered by the exploitation of geothermal energy.

5. Acknowledgments

This work has been financed by EDRA and the Regione Toscana Government Decreto n. 5859 of 07 October 2005. We do not claim that the conclusions discussed in this paper represent the position of the Regione Toscana Government on this subject. We thanks the many people at Amiata that helped us during field work, Claudio Faccenna for pointing out the fault-controlled drainage pattern at Amiata, and Guillermo Alvarado Induni for pointing out similarities between some of Amiata deposits and those emplaced by hot avalanches.

6. References

Archives of AVAM (Autorità di Vigilanza sulle Attività Minerarie), Italy, Regione Toscana, Grosseto, http://www301.regione.toscana.it/bancadati/uffici/Strutture.xml?cmu=03023, unpublished data.

A.A.V.V. 1971. La Toscana meridionale», Rend.S.I.M.P., 27.

Acocella V., 2000. Space accommodation by roof lifting during pluton emplacement at Amiata (Italy), Terra Nova, vol. 12, p. **149**-155.

Acocella V., Mulugeta G., 2000. Surface Deformation Induced by Pluton Emplacement: The Case of Amiata (Italy). Physics and Chemistry of the Earth, vol. 26, n. 4-5, p. **355**-362.

Acocella V., Behncke B., Neri M., D'Amico S., 2003. Link between major flank slip and 2002-2003. Geophysical Research Letters, vol. 30, n. 24, p. 2886-2889, doi:10.1029/2003GL018642.

Baietto A., Giudetti G., Governi S., Fusani L., Salvatici E., 2008. Shallow versus deep thermal circulations at Bagni di S. Flippo (M.te Amiata, Tuscany, Italy). Workshop: Geosciences for Geothermal Exploration: an Integrated Approach.

Batini F., Brogi A., Lazzarotto A., Liotta D., Pandeli E., 2003. Geological features of Lardarello-Travale and Mt. Amiata geothermal areas (southern Tuscany, Italy). Episodes, vol. 26, no. **3**.

Bertini G., Pandeli E., Principe C., Manzella A., 2008. Tettonica gravitativa nell'area del Monte Amiata: analisi e commenti. Rapporto interno IGG-CNR n. 10477, Pisa, Italia, 20 pages, unpublished report.

Betz A., 1962. Osservazioni Geologiche sulle ricerche minerarie per cinabro effettuate nel permesso "Le Bagnore" negli anni 1959-1961. SICEDISON s.p.a. Sezione Ricerche Minerarie – Milano. Rimin Archives, 34 pages.

686 Bird R.B., Stewart W.E., Lightfoot E.N., 1960. Transport Phenomena. John Wiley &
687 Sons, 780 pages.
688 Bonini M., Sani F., 2002, Extension and compression in the Northern Apennines
689 (Italy) hinterland: Evidence from the late Miocene-Pliocene Siena-Radicofani
690 Basin and relations with basement structures, Tectonics, vol. 21 n. 3, p. **1**-28.
691 Bonini M., Sani F., Stucchi E.M., Moratti G., Benvenuti M., Mennano G., and Tanini
692 C., 2014. Late Miocene shortening of the Northern Apennines back-arc. Journal of
693 Geodynamics, vol. 74, p. **1**-31.
694 Borgia A., Burr J., Montero W., Alvarado G.I. & Morales L.D., 1990.
695 Fault-propagation folds induced by gravitational failure and slumping of the
696 Central Costa Rica Volcanic Range: implications for large terrestrial and
697 martian volcanic edifices. Journal of Geophysical Research, vol. 95, n. B9, p.
698 **14357**-14382.
699 Borgia A., Treves B., 1992. Volcanic plates overriding the ocean crust: structure and
700 dynamics of Hawaiian volcanoes, Geological Society Special Publication vol. 60,
701 p. **277**-299.
702 Borgia A., Ferrari L., Pasquarè G., 1992. Importance of gravitational spreading in the
703 tectonic and volcanic evolution of Mount Etna. Nature, vol. 357, p. **231**-235
704 Borgia A. 1994. Dynamic basis of volcanic spreading. Journal of Geophysical
705 Research, vol. 99, p. **17791**-17804.
706 Borgia A., Delaney P.T., Denlinger R.P., 2000a, Spreading volcanoes, Annual
707 Review of Earth Planetary Sciences, vol. 28, p. **539**-70.
708 Borgia A., Lanari R., Sansosti E., Tesauro M., Berardino P., Fornaro G., Neri M.,
709 Murray J.B., 2000b. Actively growing anticlines beneath Catania form the distal
710 motion of Mount Etna's decollement measured by SAR interferometry and GPS.
711 Geophysical Research Letters, vol. 27, n. 20, p. 3409-3412.
712 Borgia A., van Wyk De Vries B., 2003, The volcano-tectonic evolution of
713 Concepción, Nicaragua, Bull. Volcanol., vol. 65, p.**248**-266.
714 Borgia A., Tizzani P., Solaro G., Manzo M., Casu F., Luongo G., Pepe A., Berardino
715 P., Fornaio F., Sansosti E., Riciardi, Fusi N., Di Donna G., Lanari R., 2005.
716 Volcanic spreading of Vesuvius, a new paradigm for interpreting its volcanic
717 activity. Geophysical Research Letters, vol. 32, L03303,
718 doi:10.1029/2004GL022155.

719 Borgia A., Grieco G., Brondi F., Badalì M., Merle O., Pasquarè G., Martelli L., di
720 Nardo T., 2006. Shale diapirism in the Quaternary tectonic evolution of the
721 Northern Apennine, Bologna, Italy. Journal of Geophysical Research, 111 (B8),
722 doi:10.1029/2004JB003375.
723 Borgia, A., 2009. Volcanic Spreading: forcing and feedback on the
724 hydrothermal system, Amiata Volcano, Italia. AGU Fall Meeting Proceedings,
725 abstract #V41A-2171.
726 Borgia A., Murray J.B., 2010. Is Tharsis Rise, Mars, a spreading volcano? Geological
727 Society of America Special Paper 470, p. **115**–122, doi: 10.1130/2010.2470(08).
728 Brogi A., 2008. The structure of the Monte Amiata volcano-geothermal area(Northern
729 Apennines, Italy): Neogene-Quaternary compression versus extension. Int. J. Earth
730 Sci. (Geol Rundsch) vol.97(4), p.**677**-703. doi: 10.1007/s00531-007-0191-1.
731 Brogi A., Fabbrini L., 2009. Extensional and strike-slip tectonics across the Monte
732 Amiata–Monte Cetona transect (Northern Apennines, Italy) and seismotectonic
733 implications. Tectonophysics vol.476: p. **95**–209; doi:10.1016/j.tecto.2009.02.020.
734 Brogi A., Liotta D., Meccheri M., Fabbrini L., 2010. Transtensional shear zones
735 controlling volcanic eruptions: the Middle Pleistocene Mt Amiata volcano (inner
736 Northern Apennines, Italy). Terra Nova, vol. 22, p.**137**-146.
737 Doi: 10.1111/j.1365-3121.2010.00927.
738 Calamai A., Cataldi R., Squarci P., Taffi L., 1970. Geology, Geophysics and
739 Hydrogeology of the Monte Amiata Geothermal Fields. Geothermics, vol.1,
740 pp.150.
741 Canuti P., Garduño V.H., Garzonio C.A., Iotti A., 1993, Slope evolution and mass
742 movements in the Mt. Amiata region (Tuscany, Italy). International Workshop on
743 environmental Volcanology, riassunto, p.**35**-36.
744 Cadoux A., Pinti D.L., 2009. Hybrid character and pre-eruptive events of Mt. Amiata
745 volcano (Italy) inferred from geochronological, petr-geochemical and isotopic
746 data. Journal of Vocanology and Geothermal Research vol.179 p.**169**-190.
747 Carmignani L., Decandia A.F., Fantozzi L.P., Lazzarotto A., Liotta D., Meccheri M.,
748 1994. Tertiary extensional tectonics in Tuscany (Northern Apennines, Italy).
749 Tectonophysics, vol.238, p.**295**-315.

750 Cataldi R., 1965. Remarks on the Geothermal Research in the Region of Monte
751 Amiata (Tuscany, Italy). Paper presented at the IAV International Symposium on
752 Volcanology (New Zealand), Nov. 1965.
753 De Castro C., 1914. Le cave di farina fossile del Bagnolo (S. Fiora) – Le Miniere
754 dell'Amiata. Memorie descrittive della Carta Geologica d'Italia, vol. 16, Roma.De
755 Delcamp A., van Wyk De Vries B., James M.R., 2008. The influence of edifice slope
756 and substrata on volcano spreading. Journal of Volcanology and Geothermal
757 Research, vol. 177, p. **925**-943.
758 Delcroix C., Brunori C., Borgia A., Vercellino A., Grico G., Moratti G., 2006. Rilievo
759 geostrutturale preliminare dell'apparato vulcanico del Monte Amiata. Regione
760 Toscana, Dec. n. 5859, pp. **46**.
761 Doveri M., Nisi B., Cerrina Feroni A., Ellero A., Menichini M., Lelli M., Masetti G.,
762 Da Prato S., Principe C., Raco B., 2012. Geological, Hydrodinamical and
763 Geochemical Features of the Volcanic Aquifer of Mt. Amiata (Tuscany, Central
764 Italy): an Overview. Acta Vulcanologica, vol. 23, n. 1-2, p. **51**-72.
765 Enel, 2009a. Concessione di Coltivazione Bagnore, Centrale geotermoelettrica
766 Bagnore 4, Integrazioni allo Studio di Impatto Ambientale, Acquiferi del Monte
767 Amiata e Coltivazione Geotermica, n. 583214, pp. **79**.
768 Enel, 2009b. Concessione di Coltivazione Piancastagnaio, Riassetto dell'area
769 geotermica di Piancastagnaio, Integrazioni allo Studio di Impatto Ambientale,
770 Acquiferi del Monte Amiata e Coltivazione Geotermica, n. 272221, pp. **77**.
771 Ferrari L., Conticelli S., Burlamacchi L., Manetti P., 1996. Volcanological Evolution
772 of the Monte Amiata, Southern Tuscany: New geological and Petrochemical data.
773 Acta Vulcanologia, vol. 8, n. 1, p. **41**-56.
774 Fink J., 1980. Surface folding and viscosity of rhyolite flows. Geology, vol. 8, p. **250**-
775 254.
776 Garzonio C.A., 2008. Paesaggi Geologici della Toscana – Regione Toscana. Pacini
777 Editore, Pisa, pp. **175**.
778 Gianelli G., Manzella A., Puxeddu M., 1997. Crustal models of the geothermal areas
779 of southern Tuscany (Italy). Tectonophysics, vol. 281, n. 3.4, p. **221**-239.
780 Girard G., van Wyk De Vries, 2005. The Managua Graben and Las Sierras-Masaya
781 volcanic complex (Nicaragua); pull-apart localization by an intrusive complex:
782 results from analogue modelling. Journal of Volcanology and Geothermal
783 Research, vol. 144, p. **37**-57.

784 Gudmuson A., 2009. Toughness and failure of volcanic edifices. Tectonophysics, vol.
785 471, p. **27**-35.
786 Holohan E.H., van Wyk de Vries B., 2008. Analogue models of caldera collapse in
787 strike-slip tectonic regimes. Bulletin of Volcanology, vol. 70, p. **773**-796.
788 Lagmay A.M.F., Valdivia W., 2006. Regional stress influence on the opening
789 direction of crater amphitheathers in Southeast Asian volcanoes. Journal of
790 Volcanology and Geothermal Research, vol. 158, p. **139**-150.
791 Leat P.T., Schmincke H.-U., 1993. Large-scale rheomorphic shear deformation
792 in Miocene peralkaline ignimbrite E, Gran Canaria. Bull. Volcanol., vol. 55,
793 p. **155**-165.
794 Le Corvec N., Walter T.R., 2009. Volcano spreading and fault interaction influenced
795 by rift zone intrusions: Insight from analogue experiments analyzed with digital
796 image correlation technique. Journal of Volcanology and Geothermal Research,
797 vol. 183, p. **170**-182.
798 Liotta D., Ranalli G., 1999. Correlation between seismic reflectivity and rehology in
799 extended lithosphere: southern Tuscany, inner Northern Apennines, Italy.
800 Tectonophysics, vol. 315, n. 1-4, p. **109**-122.
801 Linneman S.R., Borgia A., 1993. Morphology and dynamics of emplacement of
802 block lava flows at Arenal Volcano, Costa Rica. Monitoring lava flows,
803 C.R.J. Kilburn and G. Luongo Editors, UCL Press, London, p. **25**-72.
804 Mathieu L., van Wyk De Vries B., 2009. Edifice and substrata deformation induced
805 by intrusive complexes ad gravitational loading in the Mull volcano (Scotland).
806 Bulletin of Volcanology, vol. 71, p. **1133**-1148.
807 McGovern P.J., Morgan J.K., 2009. Volcanic spreading and lateral variations in
808 structure of Olympus Mons, Mars. Geology, vol. 37, n. 2, p. **139**-142.
809 Merle O., Davis G.H., Nickelsen R.P., Gourlay P.A., 1993, Relation of thin-skinned
810 thrusting of Colorado Plateau strata in southwestern Utah to Cenozoic magmatism.
811 Geological Society of America Bullettin, vol. 105, p. **387**-398.
812 Merle O., Vendeville B., 1995. Experimental modelling of thin-skinned shortening
813 around magmatic intrusions. Bulletin of Volcanology, vol. 57, p. **33**-43.
814 Merle O., Borgia A., 1996. Scaled experiments of volcanic spreading. Journal of
815 Geophysical Research, vol. 101, p. **13805**-13817.

816 Merle O., Barde-Cabusson S., Maury R.C., Legendre C., Guille G., Blais S., 2006.
817 Volcano core collapse triggered by regional faulting. Bulletin of Volcanology and
818 Geothermal Research vol.158, p. **269**-280.
819 Monaco C., Tapponnier P., Tortorici L., Gillot P.Y., 1997. Late Quaternary slip rates
820 on the Acireale-Piedimonte normal faults tectonic origin of Mt. Etna (Sicily). Earth
821 and Planetary Science Letters, vol.147 p.**125**-139.
822 Neri M., Acocella V., Behncke B., 2004. The role of the Pernicana Fault System in
823 the spreading of Mt. Etna (Italy) during the 2002-2003 eruption. Bulletin of
824 Volcanology, vol. 66, p. **417**-430.
825 Norini G., Lagmay A.M.F., 2005. Deformed symmetrical volcanoes. Geology, vol.
826 33, n. 7, p. **605**-608; doi: 10.1130/G21565.1.
827 Pandeli E., Bertini G., Castellucci P., Morelli M., Monechi S., 2005. The sub-Ligurian
828 and Ligurian units of the mt. Amiata geothermal region (south-eastern Tuscany):
829 new stratigraphic and tectonic data and insights into their relationships with the
830 Tuscan Nappe. Bollettino Società Geologica Italiana, volume speciale 3, p. **55-**71.
831 Plattern C., Amelung F., Baker S., Govers R., Poland M., 2013. The role of viscous
832 magma mush spreading in volcanic flank motion at Kilauea Volcano, Hawai'i.
833 Journal of Geophysical Research: Solid Earth, vol. 118, p.**1**-14.
834 Pompei A., 1924. Relazione sul Servizio Minerario. Biblioteca Rimin, vol. T-1281,
835 p.**132**-133.
836 Regione Toscana, 2006-2009. Carta geologica regionale, scale 1:10.000,
837 http://www.regione.toscana.it/-/carta-geologica.
838 Rovida A., Tibaldi A., 2005. Propagation of strike-slip faults across Holocene
839 volcano-sedimentary deposits, Past, Colombia. Journal of Structural Geology vol.
840 27, p. **1838**-1855.
841 Solaro G., Acocella V., Pepe S., Ruch J., Neri M., Sansosti E., 2010. Anatomy of an
842 unstable volcano from InSAR: Multiple processes affecting flank instability at Mt.
843 Etna, 1994-2008. J. Geophysical Research, vol. 115, doi:10.1029/2009JB000820
844 Suppe J., 1985. Principles of Structural Geology. Prentice-Hall, Englewood Cliffs,
845 N.J., pp 537.
846 Tibaldi A., 1996. Distinguishing tectonic faults from lava flow faults in basalts of Mt.
847 Etna and trachytes on Ischia Island, Italy. Acta Vulcanologica, vol. 8, p. **91**-98.

van Bemmelen R.W., 1949. The Geology of Indonesia.General Geology of Indonesia and Adjacent Archipelagos 1A. The Hague, The Netherlands: Government Printing Office, pp. 732.

van Wyk De Vries B., Borgia A., 1996. The role of basement in volcano deformation. In McGuire W.J., Jones A.P., Neuberg J., eds, Volcano Instabilities on Earth and other Planets, Geological Society of London Special Publication, vol. 110, p. **95**-110.

van Wyk De Vries B., Merle O., 1996. The effect of volcanic construction on rift fault patterns. Geology, vol. 24, n. 7, p. **643-**646.

van Wyk De Vries B., Matela R., 1997. Styles of volcano-induced deformation: numerical models of substratum flexure, spreading and extrusion. Journal of Volcanology and Geothermal Research, vol. 81, p. **1-**18.

van Wyk De Vries B., Merle O., 1998. Extension induced by volcanic loading in regional strike-slip zones. Geology, vol. 26, n. 11, p. **983** – 986.

Wooller L., van Wyk De Vries B., Murray J.B., Rymer H., Meyer S, 2004. Volcano spreading controlled by dipping substrata. Geology. vol. 32, n. 7, p. **573**-576.

865

866 **Table 1**. Parameters used for scaling analysis and numerical solution.

Quantity	Symbol	min. value	max. value	error
Thickness of brittle layer	H_v (m)	1000	1200	±100
	R_v (m)	5000	6000	±800
	ρ_v (kg/m^3)	2500	2700	
	s (m)	550	550	
	H_d (m)	350	350	
	ρ_d (kg/m^3)	2600	2600	
	μ_d (Pa s)	10^{18}	10^{18}	
	α	0°	5°	
	β	0°	5°	
	g (m/s^2)	9.81	9.81	
	e	0	1	

867

868

869

870 **Table 2**. Conditions explored in the solution to Eq. (6).

BC type	1^{st}		2^{nd}		3^{rd}	
Slope (α) $\Rightarrow$	$\alpha = 0°$	$\alpha = 5°$	$\alpha = 0°$	$\alpha = 5°$	$\alpha = 0°$	$\alpha = 5°$
Coefficient of topographic recovery (e) $\Downarrow$						
e = 0.00	1^{st}	1^{st}	$2^{nd} = 1^{st}$	$2^{nd} = 1^{st}$	$3^{rd} = 1^{st}$	3^{rd}
e = 0.25	1^{st}	1^{st}	$2^{nd} = 1^{st}$	$2^{nd} = 1^{st}$	$3^{rd} = 1^{st}$	3^{rd}
e = 0.50	1^{st}	1^{st}	$2^{nd} = 1^{st}$	$2^{nd} = 1^{st}$	$3^{rd} = 1^{st}$	3^{rd}
e = 1.00	1^{st}	1^{st}	$2^{nd} = 1^{st}$	$2^{nd} = 1^{st}$	$3^{rd} = 1^{st}$	3^{rd}

871

872

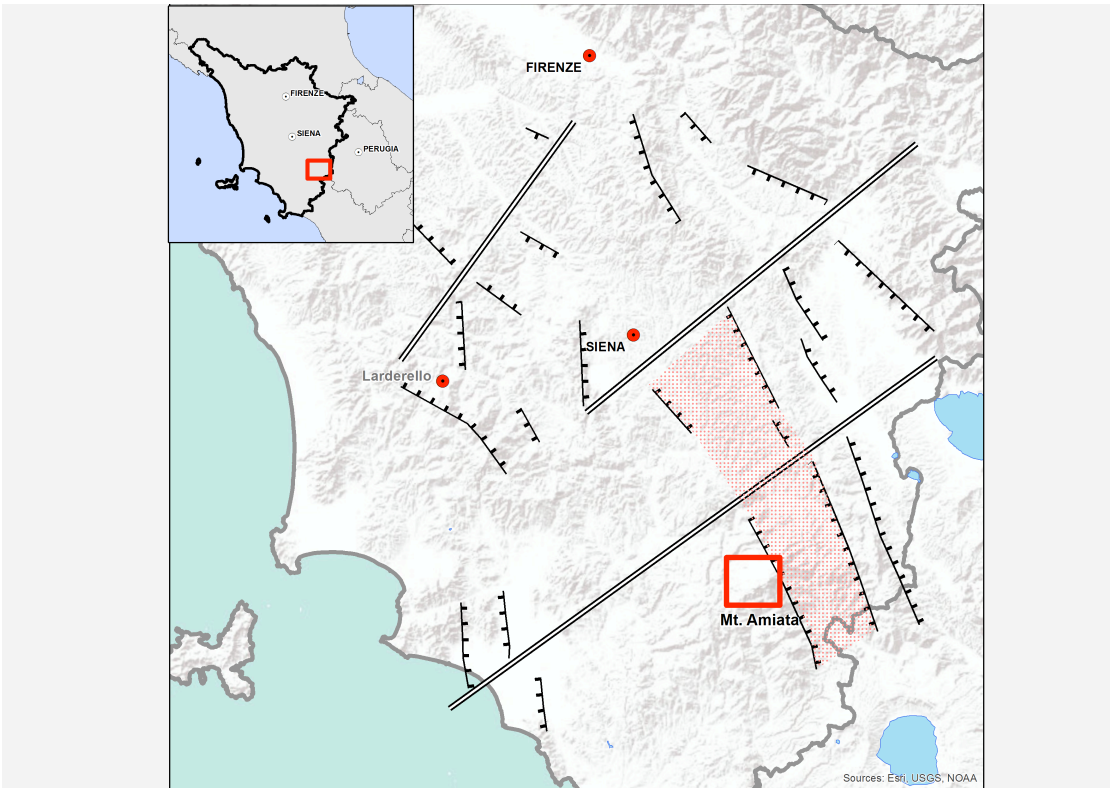

Fig. 1. Location of Amiata Volcano in relation to the extensional tectonic structures found in the back-arc of the Northern Apennines (modified after Carmignani et al., 1994). NE of Mt. Amiata. Double-lines are regional transtensional structures; ticked-lines are normal graben-bounding faults –ticks on downthrown side; pattern is the Siena-Radicofani graben. Red inset is the area of the geological map in Fig. 2.

Fig. 2. Geological map of Amiata Volcano area.

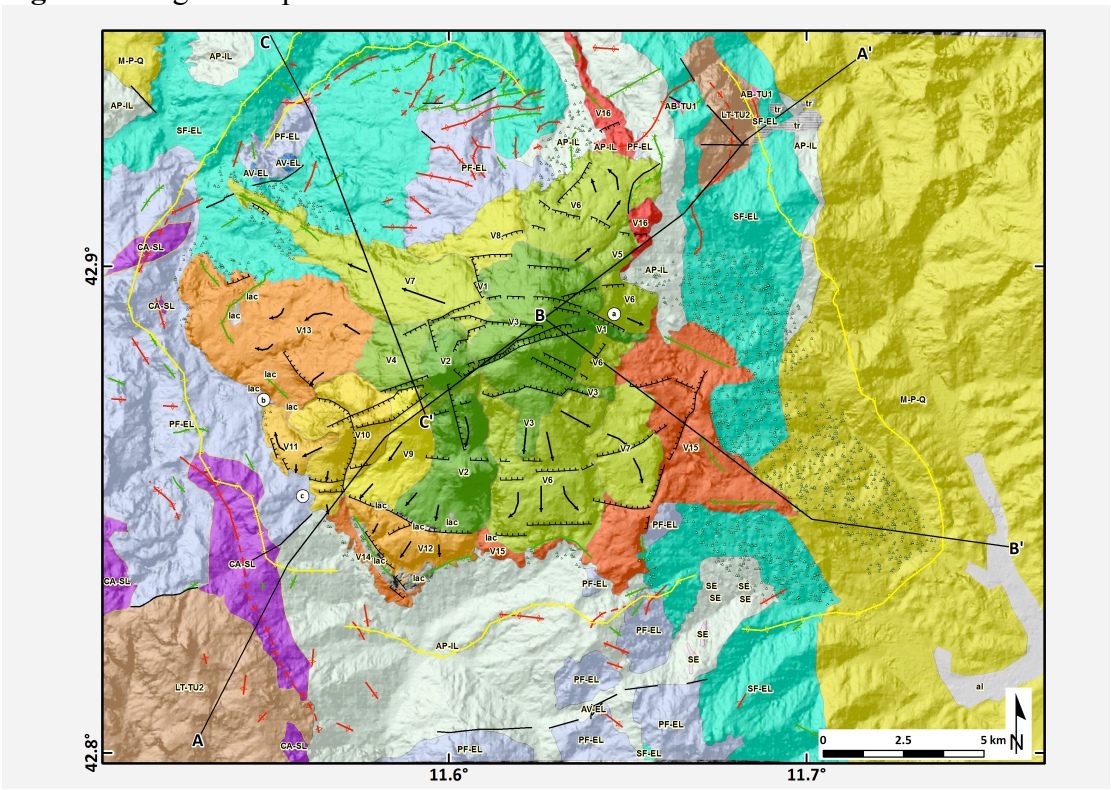

a) The geology of the volcanic units are from Ferrari et al. (1996), Regione Toscana (2006-2009), and this work. The geology of rocks forming the Amiata non volcanic-basement is from Regione Toscana (2006-2009) and this work. Note the outcrops of intrusive selagite rocks found just SE of the volcano in the Santa Fiora unit (SF-EL) that occur along the supposed uplift structure. SE and SW of Amiata between the volcano and the far edge of the uplift structures are the exploited geothermal fields. Circled A, B and C show the location of boreholes of Fig. 4.

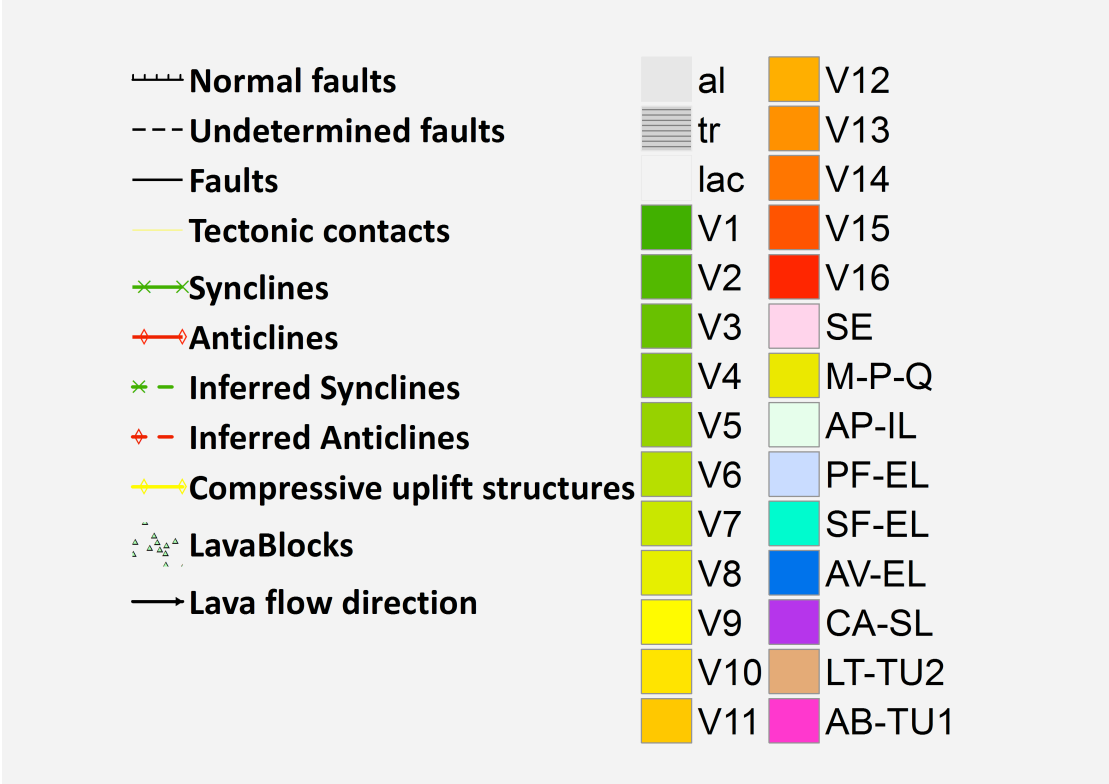

b) Legend of geological map:

- **Units V1 to V16** = identified volcanic flow units that are numbered where possible from youngest to oldest;
- SE = Selagites;
- IC = intrusive complex;
- M-P-Q = Miocene-to-Quaternary marine and continental sediments;
- IL = Internal Ligurids (AP-IL = Argille a Palombini Formation);
- EL = External Ligurian Units (AV-EL = Argille Varicolori, SF-EL = Santa Fiora Unit, PF-EL = Pietraforte);
- SL = Sub-Ligurian Units (CA-SL = Canetolo Sandstone);
- TU = Tuscan Units (AB-TU_1 = Anidriti of Burano, LT-TU_2 = carbonates and turbiditic units);
- TMC = Tuscan-Units Metamorphic Complex (MS-TMC = Micashists Group, PQ-TMC = Phyllite-Quarzite Group, and VE-TMC = Verrucano Group);
- GC = Paleozoic Gneiss upper crustal Complex.

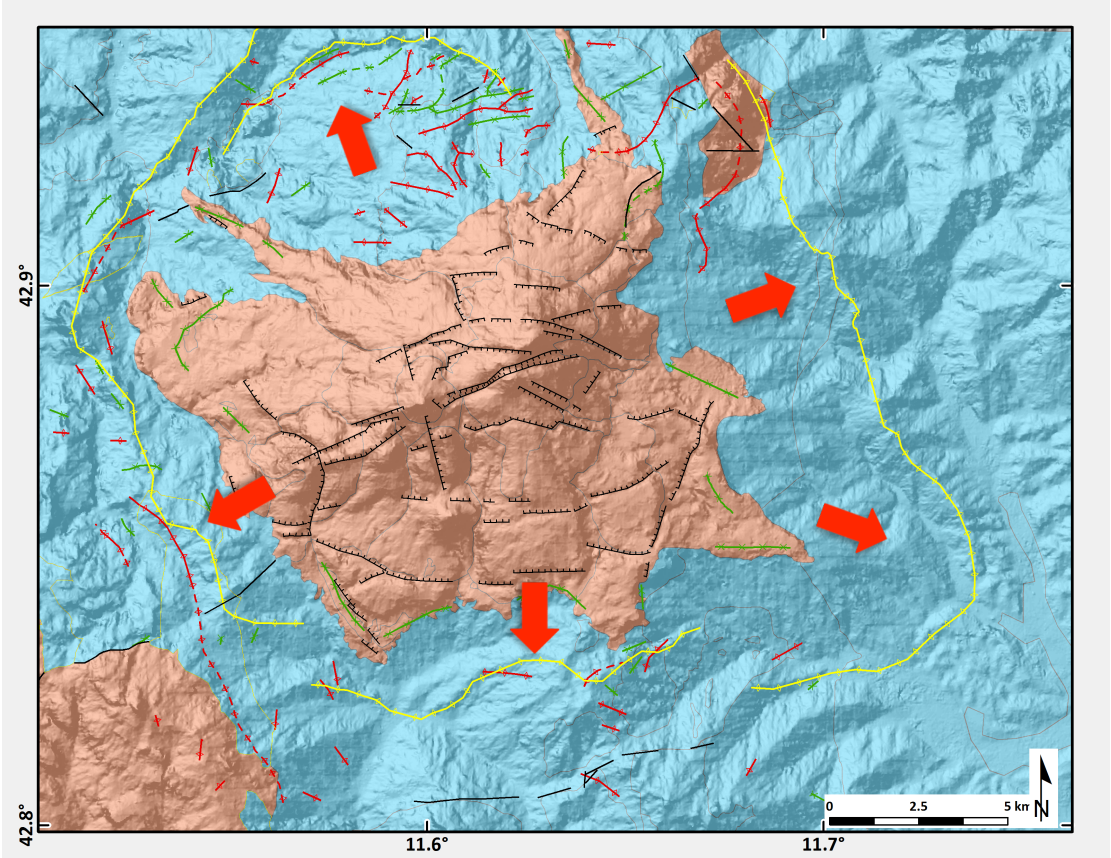

c) Sketch of spreading dynamics. Note the grabens close to the volcano summit and the folds around the periphery of the volcano. Pink = brittle units (manly Volcanic Units and Lower Tuscan Units), celeste = potentially ductile units (manly Ligurian Complex). Arrows indicate direction of spreading; other symbols are as in Fig. 2b.

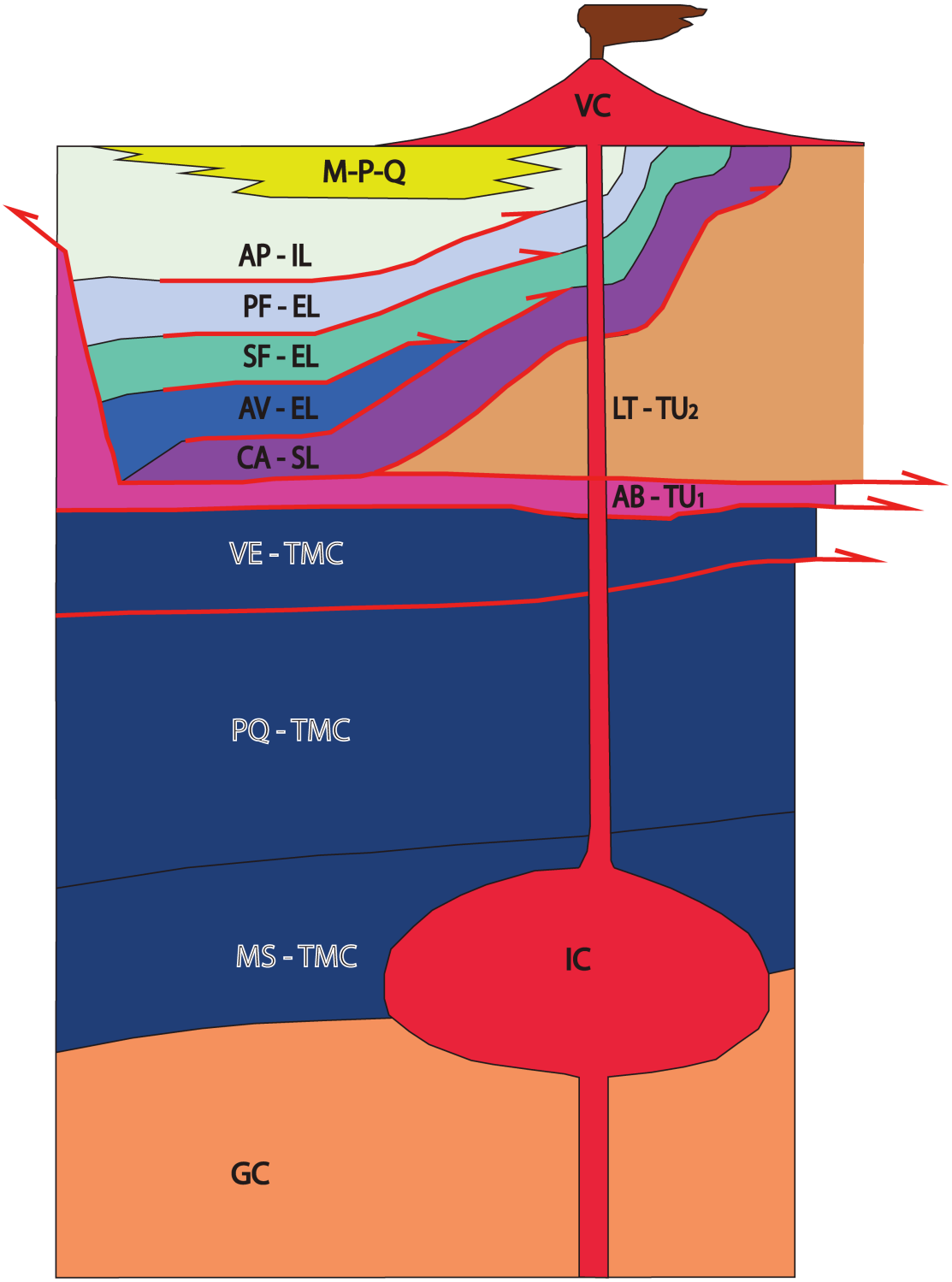

Fig. 3. Sketch of the stratigraphy of Amiata Volcano area. Acronyms and colours are in legend Fig. 2b. The volcanic units are all included into the Volcanic Complex (**VC**). Vertical and horizontal scales are arbitrary.

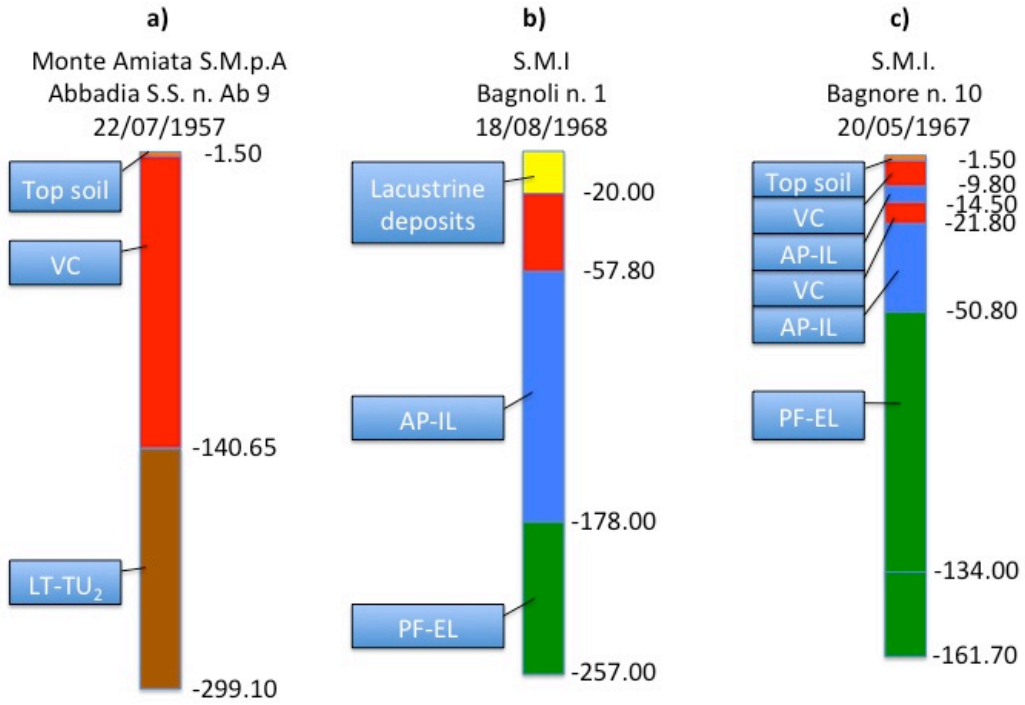

925
926
927 **Fig. 4.** Stratigraphy found in boreholes at Amiata Volcano – see Fig. 2 for borehole
928 locations. **a)** Borehole east of Amiata: note the direct contact between the lavas (**VC**)
929 and the Units of the Tuscan formation. This kind of contact offers optimal
930 hydrogeological connections between the freshwater aquifer contained in the volcanic
931 rocks above and the geothermal aquifer below. **b)** Borehole southwest of Amiata: note
932 the lacustrine deposits on top of the lava flows. These sedimentary deposits are found
933 on the volcano, wherever faults, or tilted lava flows dam the drainage. **c)** Borehole
934 south-southwest of Amiata: note that the Quaternary lavas are found within the
935 Ligurian Units of Cretaceous age (**VC** within **AP-IL**); see also Fig. 8. This type of
936 sequence is due to a structural dynamics that is younger than the lava flows. Depths
937 are meters below ground surface.
938
939

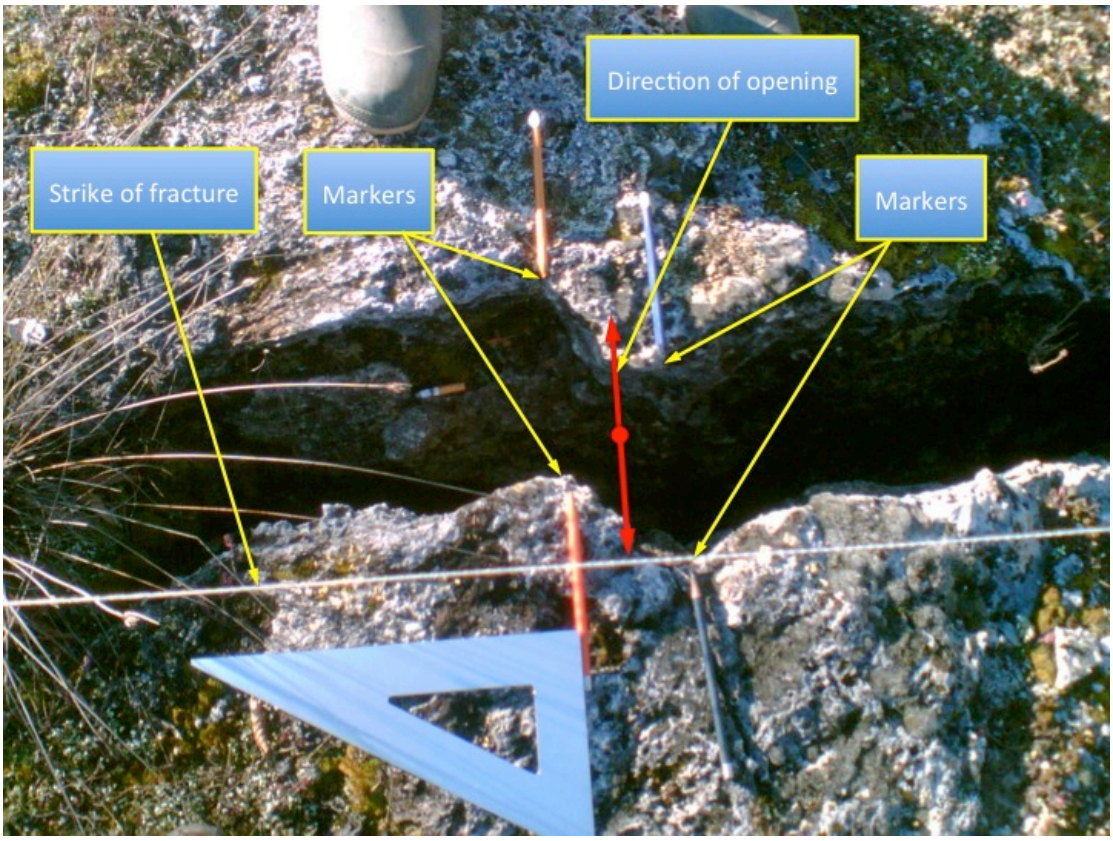

Fig. 5. Open fracture in the travertine northeast of Amiata – cf. Fig. 2a unit (**tr**). Note that, contrary to what had been previously suggested (Brogi et al., 2010), there is no strike-slip component in the approximate N-S direction of opening (red arrows) of the fracture. White line is the strike of the fracture.

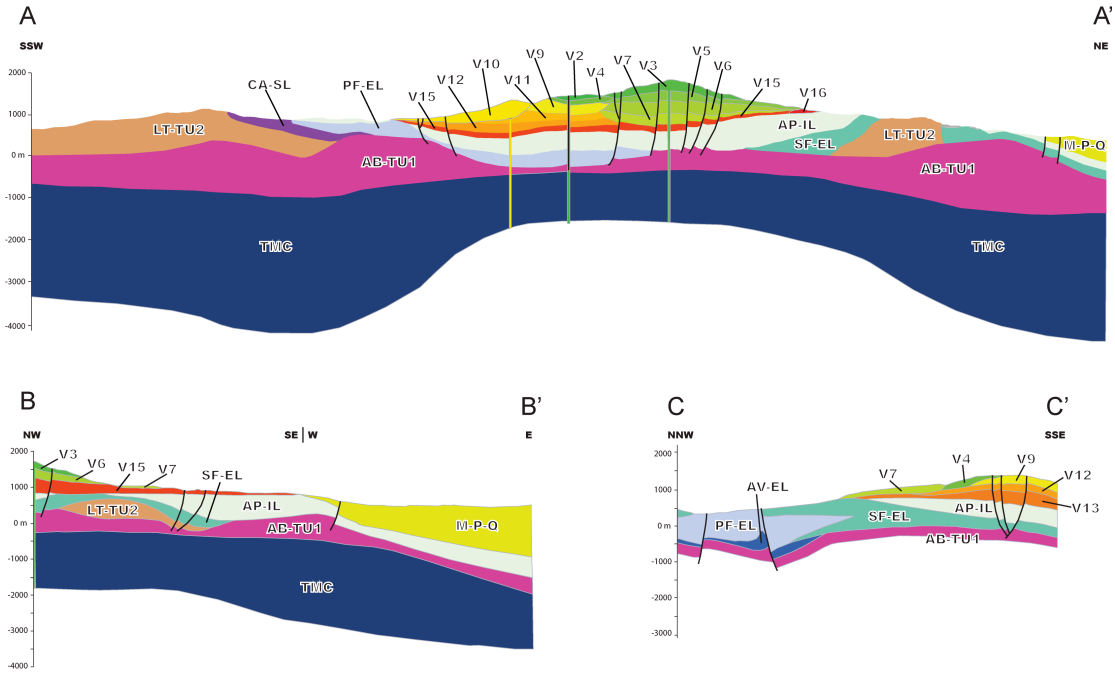

Fig. 6. Geologic cross sections of Amiata Volcano. Data from Calamai et al. (1970), Enel (2009a and b), Pandeli et al. (2005), Regione Toscana (2005-2009), and this work. Traces of cross sections are shown in Fig. 2. Section A-A' is along the ENE-WSW axis of the volcano. Section B-B' strikes from the summit of Amiata approximately ESE. Section C-C' strikes from the volcano axis NNW. Note the accumulation of anhydrites (**AB-TU$_1$**) forming domes and horsts at the base of the volcano; these domes, where covered by the clayey Ligurid rocks constitute the geothermal fields.

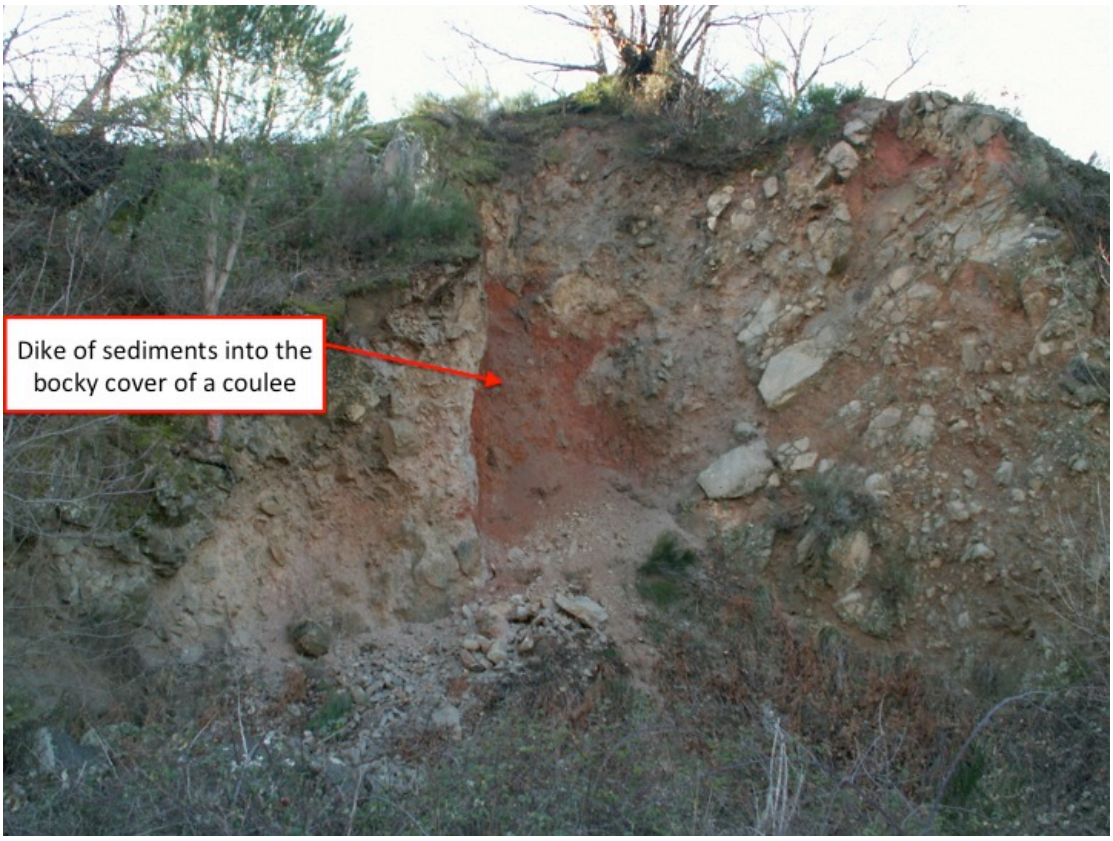

Fig. 7. Sedimentary dyke within the upper blocky section of a flow in the NW of Amiata. The clayey material is red due to heating after being entrenched in the hot flow.

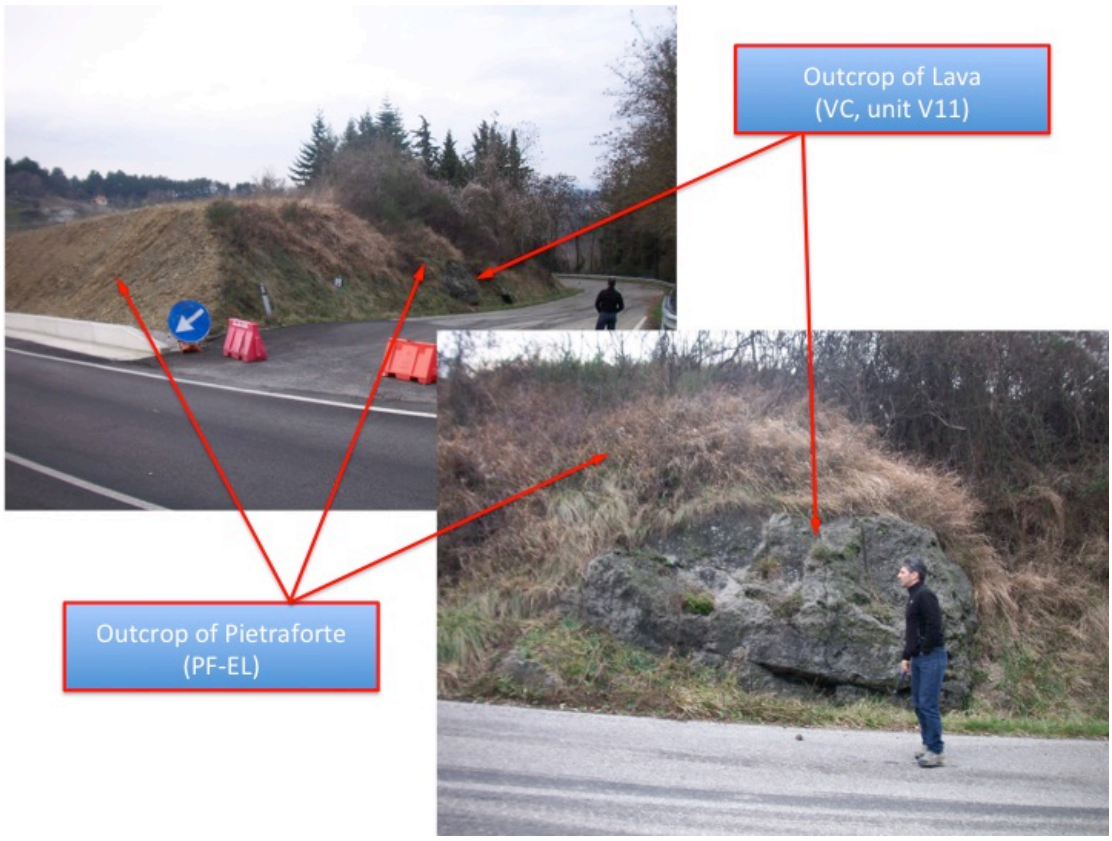

Fig. 8. One of the many outcrops of lava blocks embedded by diapiric thrusting within the Pietraforte (**PF-EL**) on the SW margin of the volcano just WNW of point (**c**) in Fig. 2a and Fig. 4 borehole (**c**).

Fig. 9. River drainage on and around Amiata Volcano.

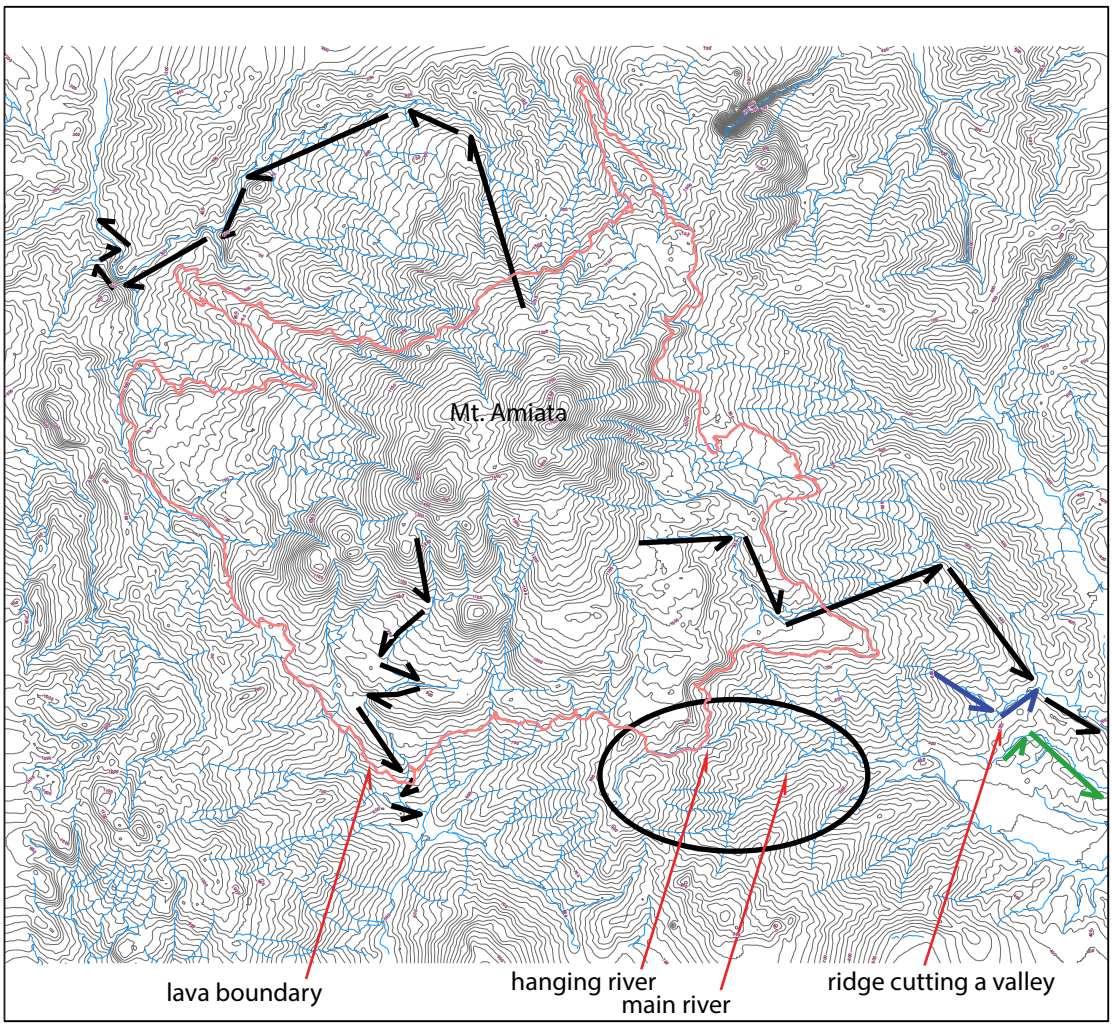

a) Highlighted with back arrows are some of the most evident angular drainage paths. The abrupt changes in flow direction are related to faults that divert the drainage. The pink line indicate the edge of the lava field.

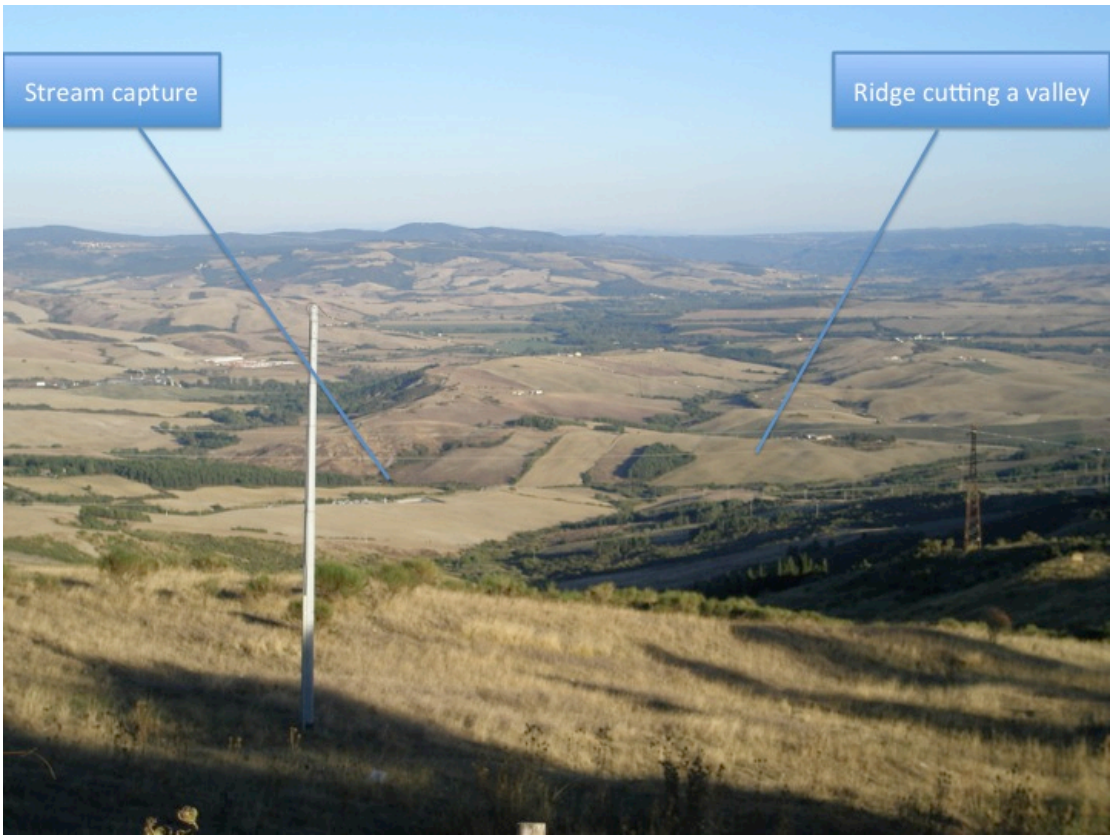

b) View, looking SW from the edge of the lava field, of the "ridge cutting a valley" shown at the bottom right of Fig. 9a.

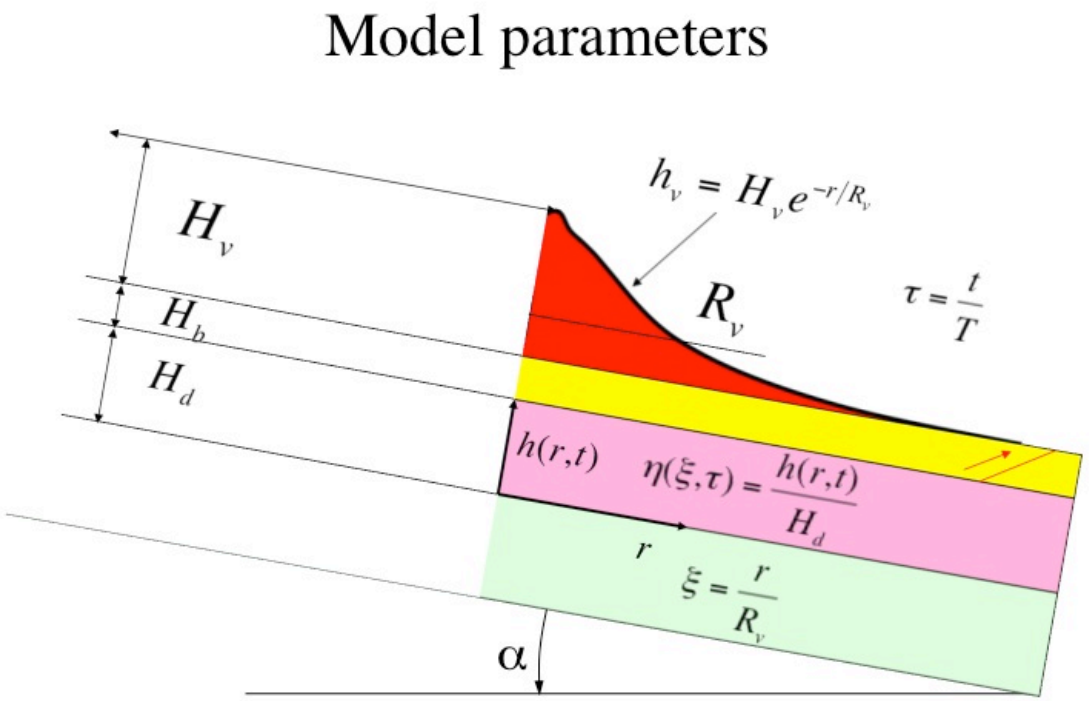

988
989
990 **Fig. 10.** Sketch of the volcano with analytical model parameters. See text for
991 explanation.
992
993

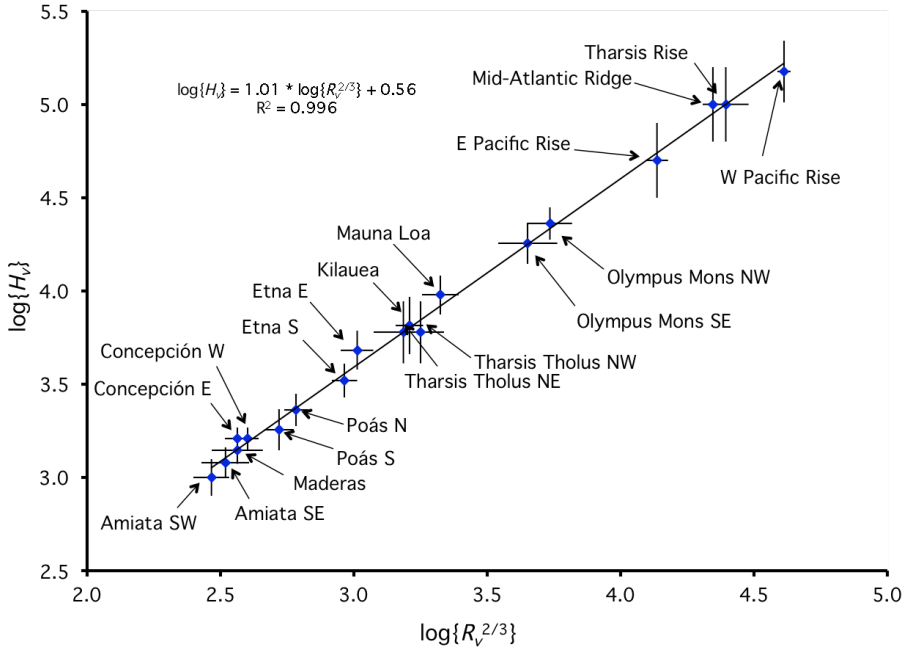

Fig. 11. The ratio between the cube of the height and the square of the length fall on a straight line as shown by Borgia and Murray (2010). Amiata Volcano falls at the lower end of the range of spreading volcanoes.

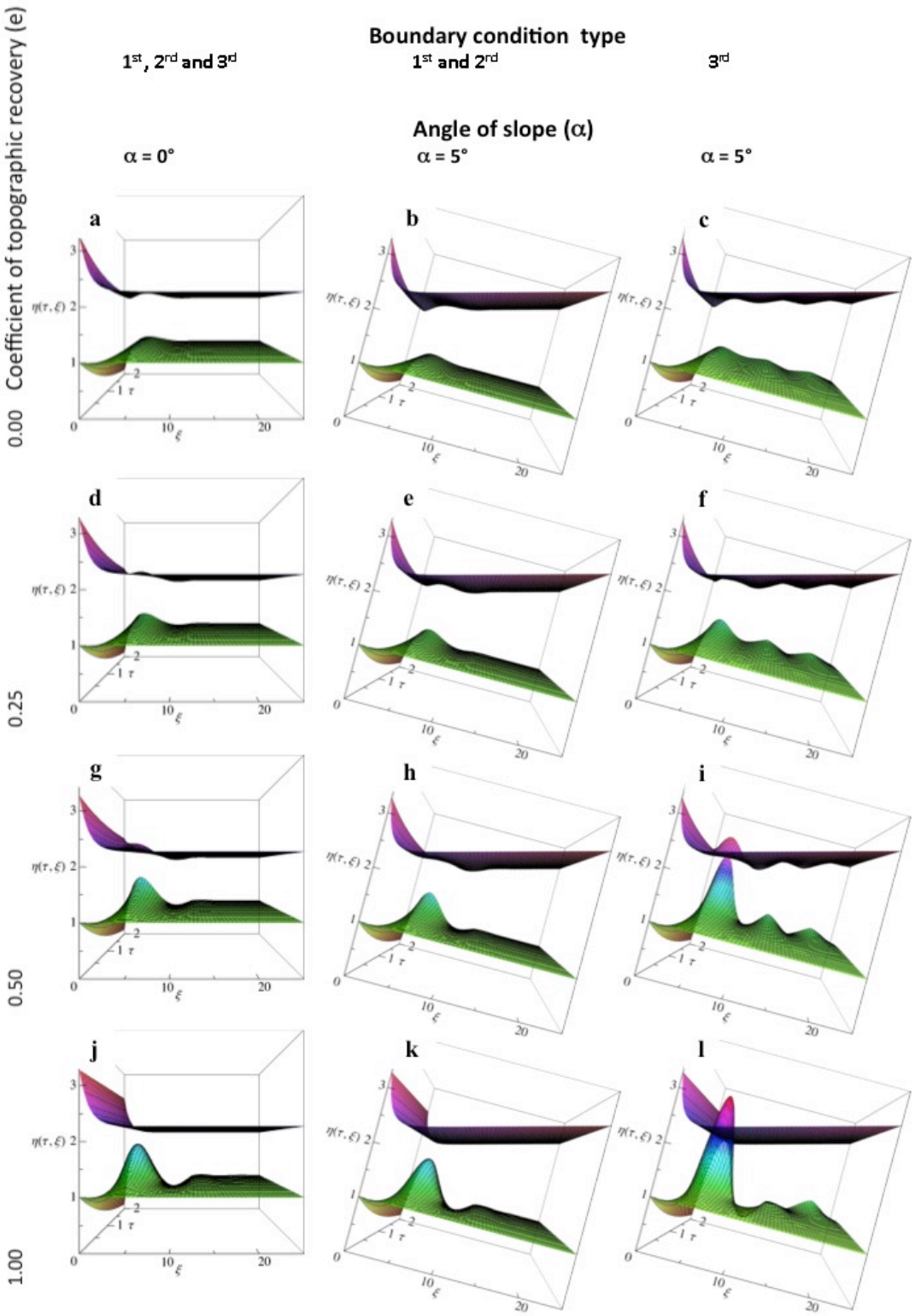

Fig. 12. Graphical representation of the solution to the Eq. 6 for various values of the parameters. ξ – the scaled radial distance from the volcanic centre – is positive to the right from $\xi = 0$ to $\xi = 25$ (in the actual model $\xi = 100$), η – the thickness of the ductile layer – is positive upward ranging from $\eta = 0$ to $\eta = 4$, and time increases into

1007 the page from $\tau = 0$ to $\tau = 2$. Therefore, on the plane ξ–η is represented the
1008 topographic profile as it evolves through time. The bottom of the box is the bottom of
1009 the ductile layer, which remains unchanged in time and space. The intermediate
1010 surface is the top of the ductile layer, which deforms as the volcano, sinking into the
1011 ductile basement, generates a wave that grows larger in time. The top surface is the
1012 topography, which show the volcano sinking into the basement as time passes. Note
1013 that as α increases and the third type of boundary condition become effective, in place
1014 of a single wave, a train of waves tend to develop. Also, as the angle of slope α and
1015 the surface erosion increase the solution evolves to a singularity: the ductile layer
1016 perches the topography. See text for a detailed explanation.